ACS ES&T Air

pubs.acs.org/estair

Article

Atmospheric Aerosol Sulfur Distribution and Speciation in Mexico City: Sulfate, Organosulfates, and Isoprene-Derived Secondary Organic Aerosol from Low NO Pathways

Madeline E. Cooke, Cara M. Waters, Joel Y. Asare, Jessica A. Mirrielees, Andrew L. Holen, Molly P. Frauenheim, Zhenfa Zhang, Avram Gold, Kerri A. Pratt, Jason D. Surratt, Luis A. Ladino, and Andrew P. Ault*

Cite This: *ACS EST Air* 2024, 1, 1037−1052

Read Online

ACCESS | Metrics & More | Article Recommendations | Supporting Information

ABSTRACT: Poor air quality is a persistent challenge in Mexico City, and addressing this issue requires an understanding of the chemical composition of $PM_{2.5}$ (particulate matter less than 2.5 μm in diameter). Sulfate and secondary organic aerosol (SOA) are two of the largest contributors to $PM_{2.5}$ in Mexico City, but uncertainties exist regarding their sources, distribution across individual particles, and ability to form organosulfates. Herein, we show using electron dispersive x-ray spectroscopy that only 41 ± 1% and 25 ± 1% of particles (aerodynamic diameter, 0.32−0.56 μm) by number at two sites in Mexico City, respectively, contain sulfur. Vibrational spectroscopy (Optical-Photothermal Infrared + Raman Microspectroscopy) shows that these sulfur-containing particles consist of inorganic sulfate (SO_4^{2-}) and organosulfates ($ROSO_3^-$). In addition, we unexpectedly measured abundant isoprene-derived SOA from low nitric oxide reaction pathways, specifically organosulfates (methyltetrol sulfates = avg. 50 ng/m^3, max. 150 ng/m^3) and polyols (methyltetrols = avg. 70 ng/m^3, max. 190 ng/m^3) using liquid chromatography with high-resolution mass spectrometry. Differences in SO_2 and NO_x concentrations between sites likely contribute to these spatial differences in sulfate, organosulfate, and SOA formation. These findings improve understanding of sulfur distribution and sources of SOA in Mexico City, which can inform efforts to improve air quality.

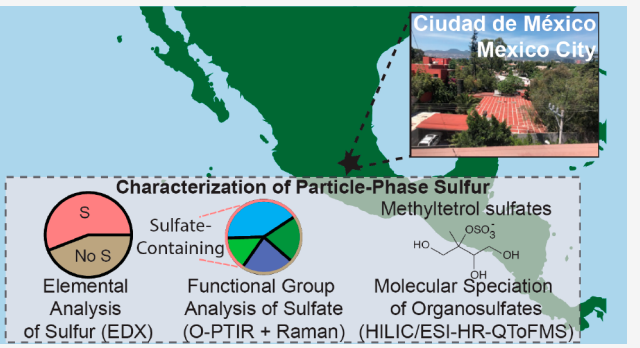

KEYWORDS: *Particulate Matter, Inorganic Sulfate, Organosulfur Species, Organic Aerosol, Single Particle Composition, Photothermal Infrared Spectroscopy, Raman Microspectroscopy, High Resolution Mass Spectrometry*

INTRODUCTION

The Mexico City Metropolitan Area is the largest megacity in North America, with a population of over 20 million people.[1] Mexico City is located at high elevation (2240 meters above sea level),[2] but is also in a basin, surrounded by mountains on three sides. The unique topography of Mexico City leads to poor air quality through the buildup of local atmospheric emissions and secondary aerosol formation (both inorganic and organic),[3] resulting in high concentrations of particulate matter (PM).[1,3]

Sulfur is a critical component of $PM_{2.5}$ (PM less than 2.5 μm in diameter) and most commonly exists as inorganic sulfate (i.e., SO_4^{2-} or HSO_4^-) or within organic species (e.g., organosulfates, $ROSO_3^-$).[4,5] Sulfate within urban PM is primarily produced from aqueous (or gas) phase oxidation of sulfur dioxide (SO_2).[6,7] Sulfate and organic components together are a significant fraction of aerosol mass globally, with sulfate typically contributing 30-60% of fine $PM_{2.5}$ mass,[8] and organic aerosol contributing up to 50% of $PM_{2.5}$ mass at continental mid-latitude sites.[9−11]

In 2006, a large-scale field campaign, the Megacity Initiative: Local and Global Research Observations or MILAGRO, was conducted to improve understanding of the emission and evolution of atmospheric pollutants in Mexico City.[12−17] The MILAGRO campaign improved understanding of sulfur and organic components within PM in Mexico City, observing that 51-55% of $PM_{2.5}$ mass in urban and industrial regions of Mexico City was carbonaceous.[14,18] The carbonaceous aerosol within $PM_{2.5}$ was found to contain both elemental and organic carbon,[19] including non-oxygenated urban primary emissions

Received: February 29, 2024
Revised: July 1, 2024
Accepted: July 2, 2024
Published: July 18, 2024

https://doi.org/10.1021/acsestair.4c00048
ACS EST Air 2024, 1, 1037−1052

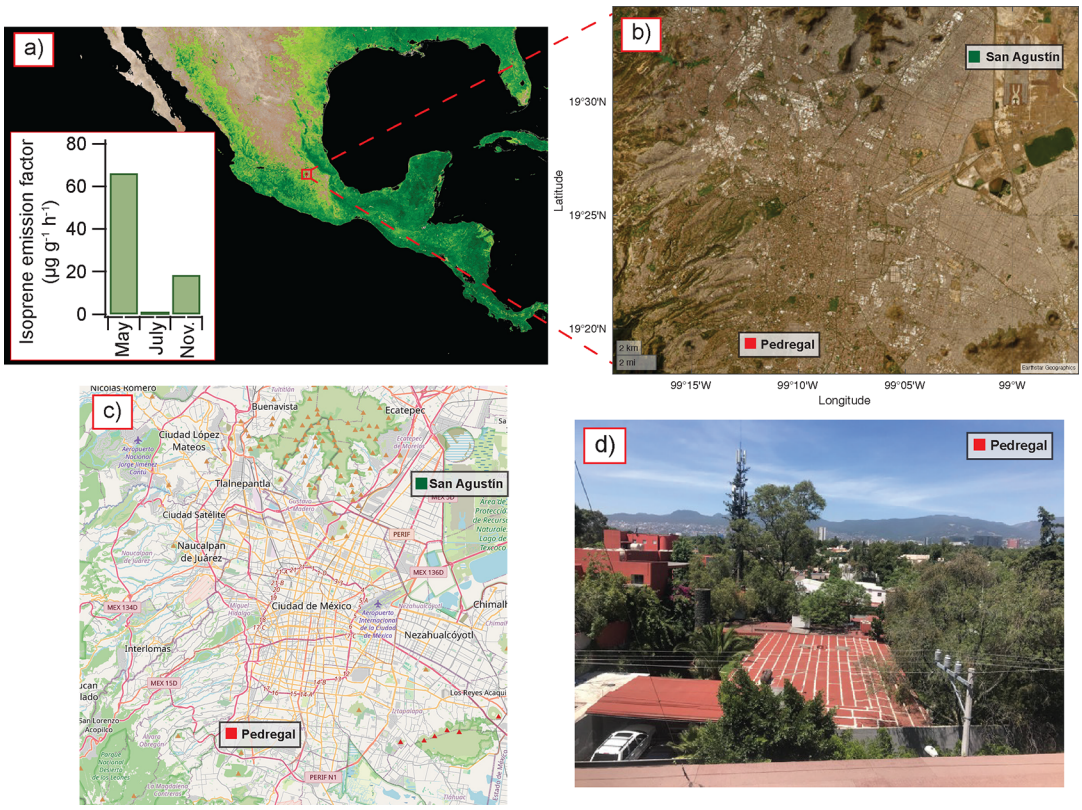

Figure 1. (a) Map of Mexico with the geographic location of Mexico City denoted by the red box (Source: NASA, https://worldview.earthdata.nasa.gov). Green colored regions on the map indicate enhanced vegetation indexes calculated with MODIS (Moderate Resolution Imaging Spectroradiometer). Inset includes isoprene emission factors determined by Dominguez-Taylor et al.[45] for Mexico City. (b) Satellite image of Mexico City basin (Satellite image courtesy of Earthstar Geographics LLC.). (c) Map of Mexico City with sampling sites shown, San Agustín (green marker) and Pedregal (red marker). Image Source: ©OpenStreetMap (https://openstreetmap.org/copyright). (d) Photograph of Pedregal sampling location.

and oxygenated organic aerosol (e.g., secondary organic aerosol or SOA).[13,17] Additionally, analysis of non-refractory PM_1 (PM less than 1 μm in diameter) showed that sulfate and organics contributed 11% and 52%, respectively, to total PM_1 mass at a supersite in northern Mexico City.[13]

Organosulfates can form within PM after the reactive uptake of less volatile oxidation products of volatile organic compounds (VOCs) to sulfate-containing particles, generating SOA.[20] Isoprene is the non-methane VOC with the highest emissions globally (~600 Tg/year),[21] and isoprene-derived methyltetrol sulfates (MTS) are one of the most atmospherically abundant organosulfate species.[22] MTS products form from the acid-driven reactive uptake of the key isoprene oxidation products, isoprene epoxydiols (IEPOX),[23] to sulfate-containing particles under low-nitric oxide (NO) conditions.[24] MTS, as well as the non-sulfated IEPOX-derived product methyltetrols (MT), contribute significantly to isoprene-derived SOA (iSOA) mass.[25−27] MTS and MT species contribute up to 58% and 34%, respectively, of lab-generated iSOA mass.[28]

Exposure to iSOA has been shown to result in adverse health effects, such as inducing oxidative stress after inhalation.[29−32] The importance of iSOA production in urban environments has been established through both field measurements[33,34] and modeling.[35−39] For example, in Atlanta, GA, iSOA represents 33% of non-refractory PM_1 mass, as determined by source apportionment of real-time aerosol mass spectrometry using positive matrix factorization.[36] iSOA production and properties are highly influenced by anthropogenic emissions (e.g., SO_2 or nitrogen oxides, NO_x)[40] and isoprene emissions from terrestrial vegetation, with many studies focused on regions with very high isoprene concentrations (e.g., Atlanta, USA,[36] and Manaus, Brazil[28,41]).

During the MILAGRO campaign, SOA represented a significant fraction of total organic aerosol mass.[13,42] Aiken et al.[13] found that SOA represented almost half of the non-refractory organic aerosol mass on average from measurements using real-time high-resolution aerosol mass spectrometry (HR-AMS). Stone et al.[42] concluded that SOA represented 20-25% of total organic carbon mass, as determined from $PM_{2.5}$ filter samples measured by gas chromatography interfaced to mass spectrometry. To further investigate SOA composition, authentic standards for two organosulfates (i.e., glycolic acid sulfate and lactic acid sulfate) were developed and their mass concentration was determined at two MILAGRO sampling sites, finding that the mass concentration of these species was comparable to other measurements globally such as in Riverside and Bakersfield, CA.[43]

During the 2006 MILAGRO campaign, it was found that the SOA was primarily from VOCs of an anthropogenic origin,[42] and that biogenic VOCs were insignificant contributors to SOA formation.[44] However, isoprene emissions from net-leaf oak trees in Mexico City are estimated to range from 1.9 $\mu g\ g^{-1}\ h^{-1}$ to 66.27 $\mu g\ g^{-1}\ h^{-1}$, depending on the season,[45] and could potentially be a source of iSOA in the city. Due to a lack of synthetic standards and analytical techniques available at the

https://doi.org/10.1021/acsestair.4c00048
ACS EST Air 2024, 1, 1037−1052

time, the mass concentration of many important iSOA products, including the organosulfate species MTS, were not quantified in PM samples from the MILAGRO campaign. Thus, the contribution of iSOA to organic aerosol in Mexico City remains unresolved.

While sulfur is abundant within $PM_{2.5}$, it is not frequently present in every aerosol particle.[46,47] Single particle measurements are thus key to understanding the composition and source of sulfur, including both particle-phase inorganic sulfate and organosulfate formation, and to fully characterizing an aerosol population. Single-particle microscopic measurements from the MILAGRO campaign showed that carbon is frequently mixed with inorganic components (S, N, O, P)[15] and industrial emissions (Zn, Pb, Cl).[16] Additional single-particle measurements using the aerosol time-of-flight mass spectrometer revealed that submicron aerosol was largely comprised of aged organic aerosol and biomass burning aerosol, as well as showing that aged oxidized organic aerosol was mixed with sulfate.[17] While important insights into $PM_{2.5}$ sources and aging in Mexico City have been gained with these previous single-particle analyses, newer analytical capabilities for individual particle analysis,[48−51] including the development of the optical photothermal infrared spectrometer (O-PTIR) which allows for simultaneous collection of Raman and Infrared spectra, enable a deeper understanding of sulfur speciation and distribution within $PM_{2.5}$. Additionally, the development of authentic standards as well as improved methodology for separation of iSOA species, specifically hydrophilic interaction liquid chromatography coupled with electrospray ionization high-resolution quadrupole time-of-flight mass spectrometry (HILIC/ESI-HR-QTOFMS),[28] now enable the robust quantification organosulfates in SOA.[52] More single-particle analysis is needed as the climate and health impacts of aerosols are largely driven by single particle composition and physical properties (size, optical properties, hygroscopicity, etc.).[53−55]

Characterizing the distribution of sulfur, organosulfates, and iSOA within single particles in Mexico City $PM_{2.5}$ is important to improve understanding of aerosol sources and formation mechanisms. Herein, we combine single-particle compositional analysis with speciated measurements of iSOA to understand $PM_{2.5}$ composition at two sites with differing SO_2 and NO_x concentrations within northern and southern Mexico City during May − June 2018. We use computer-controlled scanning electron microscopy coupled with electron dispersive x-ray spectroscopy (CCSEM-EDX) to sort the aerosol population into the five most abundant categories of aerosol particles by elemental composition and identify sulfur-containing particles. We then use optical photothermal infrared (O-PTIR) + Raman microspectroscopy to quantify the number fractions of particles in each category containing sulfate, organosulfates, soot, and/or organic carbon. Finally, we quantify the mass concentrations of the iSOA products MTS and MT from low-NO chemical pathways and explore the formation of additional iSOA products using HILIC/ESI-HR-QTOFMS. The results below improve our understanding of the interplay between sulfur and organic species and the abundance of low-NO iSOA products in a densely populated urban environment.

MATERIALS AND METHODS

Description of Sites. Aerosol particle samples were collected in summer 2018 from two sites in Mexico City, Mexico: Pedregal in the south (19°19'30.9" N, 99°12'13.4" W) and San Agustín in the north (19°31'59.7" N, 99°01'48.4" W) (Figure 1a-d). The San Agustín site is a densely populated urban zone with high industrial activity, and the Pedregal site is primarily a residential zone containing vegetation and low traffic activity.[56] Both sites are Automatic Atmospheric Monitoring Network (RAMA, by acronym in Spanish for Red Automática de Monitoreo Atmosférico) government monitoring stations. Ambient concentrations of O_3, SO_2, and NO_x ($NO + NO_2$), as well as the meteorological conditions (temperature and relative humidity, RH), are continuously monitored at the RAMA stations. A detailed comparison of environmental conditions at the two monitoring sites is provided in the discussion section as well as in the supplemental information. This includes a comparison of the NO, nitrogen dioxide (NO_2), and NO_x ($NO + NO_2$) for the entire sampling period at the two sites (Figure S1); temperature and RH for the two sampling days (Figure S2); as well as a comparison of the temperature and RH for the entire sampling period at both sites (Figure S3 and S4, respectively).

Regional emissions in Mexico City include both anthropogenic (vehicular emissions, cooking, oil refineries, and other industrial activities) and natural sources (vegetation, volcanic emissions).[14] Primary sources of sulfur in Mexico City are the active Popocatépetl volcano, which is located ~81 km to the east of Mexico City, and Tula-Vito-Apasco region, which is an industrial zone located to the north of Mexico City containing oil refineries, cement industries, and powerplants.[57] Biogenic emissions in Mexico City include isoprene, and estimated seasonal emission factors of isoprene based on common plant types are shown in Figure 1a.[45]

Description of Sample Collection. In this study, six samples were collected at each location between the dates of 5/30/2018 to 6/11/2018 (Pedregal location) and 6/18/2018 to 6/26/2018 (San Agustín location). The dates and locations of all samples are detailed in Table S1. For each date, sampling was conducted for a 24-h period from 12 PM to 12 PM local time. Aerosol particles were collected using a microorifice uniform deposit impactor (MOUDI) via impaction onto aluminum foil (TSI Aluminum Foil Substrates for MOUDI, 47 mm diameter) and quartz substrates (Ted Pella Inc.) on MOUDI stages 6 and 7 (aerodynamic diameter (d_a) ranges of 0.32−0.56 μm and 0.18−0.32 μm, respectively) for offline microscopy/spectroscopy analysis. MOUDI samples were sealed with parafilm and stored in the dark at room temperature until later analysis (over multiple years). Storage procedure followed Laskina et al.[58] to prevent the degradation of sample chemical composition and particle morphology. Aerosol particles were also sampled onto quartz filters (Pallflex membrane filters, 47 mm diameter) using a MiniVol Portable Sampler (Airmetrics) at 5 L/min for offline chromatography/mass spectrometry analysis. The filters were stored in the dark for four years at -20 °C before extraction using a previously described procedure.[28] The stability of iSOA species within $PM_{2.5}$ filter samples stored for several years under these conditions has been previously demonstrated.[59]

Aerosol Particle Analysis. CCSEM-EDX was used to determine the particle types[46,60−65] present for two case study sampling days, Pedregal 6/11/2018 (1899 particles analyzed) and San Agustín 6/18/2018 (1313 particles analyzed). For both case study days, a sample from stage 6 of the MOUDI (d_a, 0.32−0.56 μm) was analyzed. CCSEM-EDX was

https://doi.org/10.1021/acsestair.4c00048
ACS EST Air 2024, 1, 1037−1052

conducted using a FEI Helios Nanolab SEM/FIB (EDAX Inc.), as described previously.[66] X-ray spectra were analyzed for the elements C, O, Si, Na, P, S, Ca, K, Fe, and Cu. The instrument was operated in secondary electron mode with an accelerating voltage of 20.0 kV and a current of 0.43 nA. The particles were sorted into particle classes using a rule-based classification approach,[15,16,67] based on the presence of peaks associated with key elements in each particle class, with the criteria detailed in Figure S5.

Simultaneous O-PTIR and Raman microspectroscopy (O-PTIR+Raman) of individual particles was conducted on the samples from the case study days to characterize the carbonaceous particles, which were further sorted into organic and soot categories based on the functional groups present in each particle. It should be noted that it is possible that the degradation of organosulfur could occur during sample storage (i.e., hydrolysis of organosulfate compounds), and thus the number fraction of organic particles observed in this study should be treated as a lower bound. The two case study days described above were analyzed: Pedregal 6/11/2018 (95 particles analyzed) and San Agustín 6/18/2018 (102 particles analyzed). O-PTIR was conducted using a mIRage instrument (Photothermal Spectroscopy Corp.) that simultaneously collects IR and Raman spectra of an individual particle, as previously described.[48] Briefly, O-PTIR uses both a tunable IR laser (QCL, MIRcat-QT, spectral range of 950−1800 cm^{-1} and 2700−3000 cm^{-1}) and continuous wave visible laser (532 nm), co-aligned through a Cassegrain objective (40 ×, 0.78 N.A.). The IR laser scans from low to high energy, and when a species in the particle absorbs at a specific frequency a photothermal expansion and change in refractive index leads to increased scattering of the visible laser, which is recorded with a photodiode detector. The IR spectra were collected with six averages using an IR power of 24%, probe power of 5%, and 2× detector gain. IR spectra were collected with a spectral resolution of 2 cm^{-1} and a sweep speed of 1000 cm^{-1}/s. Raman spectra were collected with six averages and an integration time of 10 s. Raman spectra were collected using a Horiba iHR320 module with a grating of 600 grooves/mm and spectral resolution of 4 cm^{-1}.

Filter extracts were analyzed for all sampling days using HILIC/ESI-HR-QTOFMS operated in the negative (−) ion mode using a previously described method,[28] including quantifying the particulate mass of MTS and MT compounds on the filter samples. Briefly, filters were immersed in 8 mL of methanol and extracted with 50 min of ultrasonication. The extracts were then syringe filtered (Agilent Premium Syringe Filter, PTFE, 4 mm diameter, 0.2-μm pore size), and the solvent was subsequently evaporated using high-purity nitrogen gas. The dry extract was resuspended in 95:5 acetonitrile (ACN, Fischer Scientific, HPLC Grade): Milli-Q water (18.2 MΩ cm^{-1}). A 5-μL aliquot of each filter extract was injected onto the HILIC column and analyzed following the method previously described.[68] HILIC separations were conducted using a Waters Acquity UPLC BEH Amide column (2.1 × 100 mm, 1.7-μm particle size) with mobile phase A (0.1% ammonium acetate in water, adjusted to pH 9) and mobile phase B (0.1% ammonium acetate in 95:5 ACN:Milli-Q water, adjusted to pH 9) with a gradient as described previously.[68] Authentic standards of MTS and MT were synthesized as described previously,[28] and calibration curves of both standards were prepared ranging from 0.5 to 100 ppm in order to quantify their mass in filter extracts. The limit of quantification (LOQ) for this method is as previously reported (LOQ for MTS = 5.75 μg/L or 0.2 ng/m^3 and LOQ for MT = 25.8 μg/L or 1.0 ng/m^3).[28] The LOQ and LOD for each sample is converted to mass concentration by considering the theoretical mass concentration for a sample at the LOD and LOQ based on the average extraction efficiency (55 ± 8%) for all samples. All of the samples analyzed in this data set were above the LOQ for both species except for the sample collected at San Agustín on 6/18/2018.

HYSPLIT Analysis. The sources of the air masses sampled for all measurement days at the Pedregal and San Agustín location were determined using the National Oceanic and Atmosphere Administration Hybrid Single-Particle Lagrangian Integrated Trajectory (NOAA HYSPLIT) back trajectory model.[69] For each run, the backward air mass trajectory for each field site location was calculated using GDAS (1-degree, global, 2006-present) at heights of 100, 200, and 500 m for a duration of 48 h. It should be noted that the 1-degree spatial resolution of HYSPLIT may not capture all transport patterns at the sampling locations, and this uncertainty should be considered when interpreting the modeling results.

RESULTS AND DISCUSSION

Case Study Days for Single Particle Analysis. Two case study days were selected for single particle analysis based on ambient data from the RAMA monitoring network, specifically

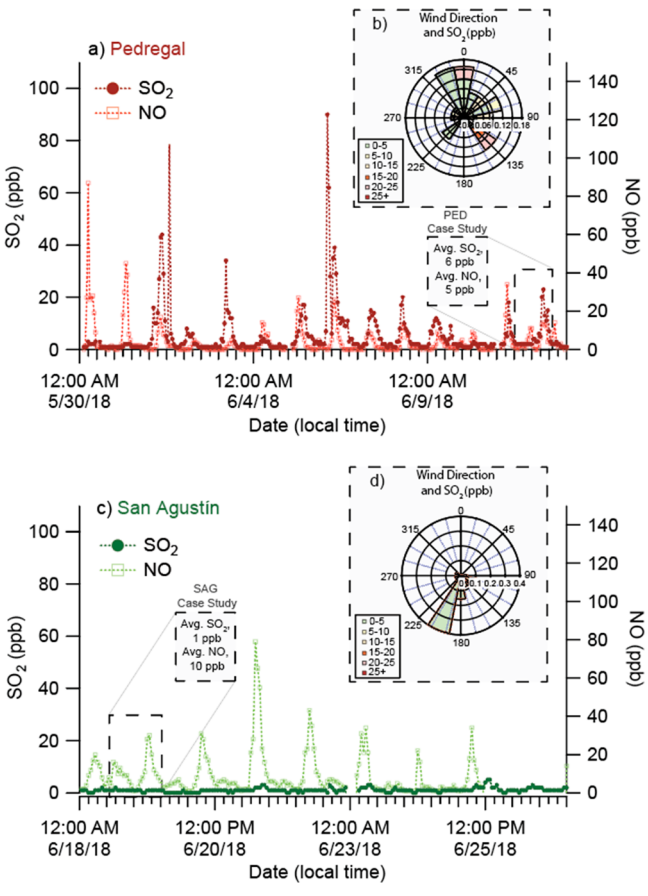

Figure 2. SO_2 (ppbv) and NO (ppbv) at (a) Pedregal and (c) San Agustín field sites measured by the RAMA government monitoring station. Rose plots provide wind direction and concentration for SO_2 during case study days for (b) Pedregal 6/11/2018 and (d) San Agustín on 6/18/2018.

https://doi.org/10.1021/acsestair.4c00048
ACS EST Air 2024, 1, 1037−1052

SO_2 and NO (Figure 2), with the Pedregal case study day chosen as a representative of overall high-SO_2 and high-NO conditions and the San Agustín case study day as representative of overall low-SO_2 and high-NO conditions. NO_2 and NO_x concentrations are provided separately in Figure S1 for comparison. SO_2 at the Pedregal site averaged 6 ppbv (max. 90 ppbv), which was higher than the average 1 ppbv (5 ppbv max) at the San Agustín site. In contrast to SO_2, the NO levels were higher at the San Agustín site (avg. 9 ppbv and max. 79 ppbv) than the Pedregal site (avg. 3 ppbv and max. 45 ppbv). The NO concentration at both sites was mostly low (below 10 ppbv) throughout the sampling period (88% of the time at Pedregal and 73% at San Agustín below 10 ppbv), indicating low NO conditions,[70] which impact the reactions mechanisms that are important for the iSOA formation discussed below. HYSPLIT analysis indicated that polluted air masses were not transported from beyond or across the basin (Figures S9−S20) at both sites. This means that differences in SO_2 and NO concentrations were likely driven by local emissions, such as the industrial emissions at the San Agustín site or vehicular emissions at the residential Pedregal site. Though both sites were typically under low NO conditions, Pedregal had much higher SO_2 concentrations.

The case study day for the Pedregal site was 6/11/2018 and for the San Agustín site was 06/18/2018, and these specific days are hereafter referred to as PED and SAG (Figure 2a,b and 2c,d). The case study days were representative of the overall sampling period with higher NO concentrations at SAG (range 1−30 ppb; avg. 10 ppb) than at PED (range not detected (n.d.) − 14 ppb; avg. 5 ppb), but higher SO_2 levels at PED (range 2−23 ppb; avg. 6 ppb) than SAG (range n.d. − 2 ppb; avg. 1 ppb). The wind direction and ambient concentration of SO_2 for these case study days are provided in Figures 2b (PED) and 2d (SAG). The higher SO_2 at PED is reflected in the observations of greater particle-phase sulfur, which is discussed further below.

Description of the Particle Classes Identified. To better understand the influence of SO_2 on particle composition, individual particles (d_a, 0.32-0.56 μm) within $PM_{2.5}$ from each case study day were analyzed using CCSEM-EDX. Five main types of particles were identified across the two case study days based on the elemental composition: carbonaceous (which can include both organic carbon and soot, as these are not differentiated using EDX),[46,63,71,72] Ca-rich,[67,73−75] Si-rich,[67,74,75] Fe-rich,[64,67,74] and biological.[46,76] Figure 3 shows representative single-particle EDX spectra and corresponding SEM images for each of these most abundant particle types. Based on spreading upon impaction, projected area diameters (d_{pa}) in the images of Figure 3 are larger than aerodynamic diameters.[77,78]

The carbonaceous particles were classified based on the presence of an intense carbon peak. Carbon-rich particles containing P and/or Ca peaks were not included in the carbonaceous particle group; they were instead classified as biological or Ca-rich particles, respectively. The carbonaceous particles in this study are likely a combination of primary and secondary organic carbon,[79−81] as well as soot[81,82] from combustion (both fossil fuels and biomass burning), as CCSEM-EDX is unable to easily distinguish between these categories (see O-PTIR+Raman below). Overall, slightly less than half of the measured carbonaceous particles contained S > 2 mol % (40 ± 1% by number),[80] and the speciation of these S-containing inorganic and organic compounds is explored in more detail below. In addition to S, some carbonaceous particles were observed to be mixed with O, Fe, Na, Si, K, Ti, and for Cu, indicative of industrial, biomass burning, other combustion processes, mineral dust, or dry lake beds.[17]

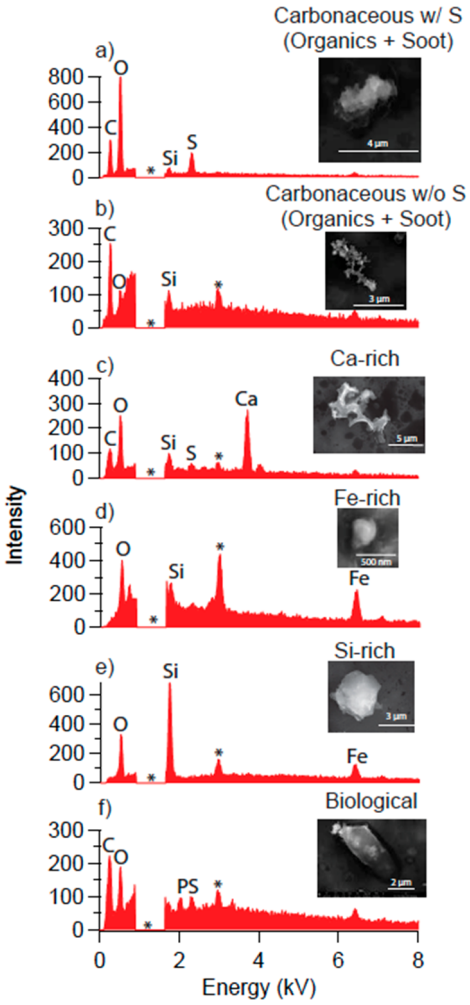

Figure 3. Example EDX spectra and SEM images for the most abundant particle classes: (a) Carbonaceous with Sulfur; (b) Carbonaceous without Sulfur; (c) Ca-rich; (d) Fe-rich; (e) Si-rich; and (f) Biological. Projected area diameter reflects spreading on substrate, which represents between a 4:1 and 10:1 ratio with aerodynamic diameter.[75,76] Asterisks designates peaks resulting from aluminum foil background. The large Al background peak from 0.9 to 1.64 kV has been zeroed and the other peaks with asterisks denote the summed aluminum peak. Carbonaceous with Sulfur, Carbonaceous without Sulfur, Fe-rich, and Si-rich particle classes are from samples collected on Stage 6 of the MOUDI (d_a = 0.32-0.56 μm), and Ca-rich and biological particle classes are from samples collected on Stage 7 of the MOUDI (d_{50} = 0.18-0.32 μm). Carbonaceous particle classes include soot particles, as EDX cannot easily differentiate them.

These SEM-EDX results are largely consistent with carbonaceous particles observed in Mexico City and previously characterized using SEM-EDX from three sites during MILAGRO 2006, including one site within the city center and two sites located northeast of the city (~29 and 65 km from the center).[15] An additional study also observed carbonaceous particles mixed with S, N, O, K, and Na, in addition to a large fraction of biomass burning particles as measured by single-particle mass spectrometry.[17]

https://doi.org/10.1021/acsestair.4c00048
ACS EST Air 2024, 1, 1037−1052

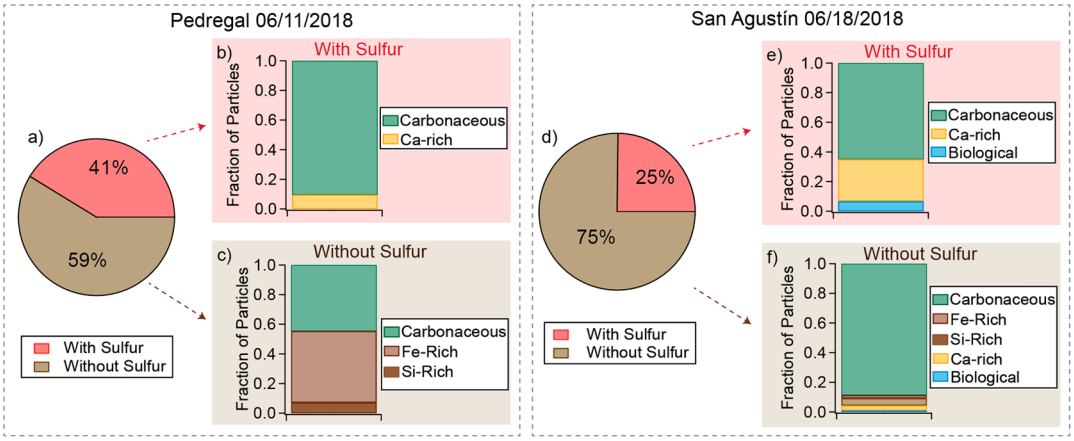

Figure 4. Number fraction of particle type as determined by CCSEM-EDX analysis for the Pedregal 6/11/2018 (1899 particles) sample and the San Agustín 6/18/2018 (1350 particles) sample. Both samples were collected on stage 6 of the MOUDI (d_a = 0.32−0.56 μm). Pie charts represent total number fraction of particles in (a) Pedregal 6/11/2018 sample and (d) San Agustín 6/18/2018 sample with and without the presence of a sulfur peak (S > 2 mol%). Bar graphs represent the number fraction of each particle type within these categories: (b) Pedregal 6/11/2018 particle classes with sulfur, (c) Pedregal 6/11/2018 particle classes without sulfur, (e) San Agustín 6/18/2018 particle classes with sulfur, and (f) San Agustín 6/18/2018 particle classes without sulfur.

In addition to carbonaceous particles, several different types of dust were observed including Ca-rich, Si-rich, and Fe-rich particles. These include natural mineral dusts and dust/fly ash formed from anthropogenic processes (e.g., steel production, cement production).[64,74] The Si-rich and Fe-rich particles were classified based on the largest peak (i.e., Si-rich particles contained a Si peak ≫ Fe peak and vice versa). No particles in the Fe-rich and Si-rich categories contained Ca peaks. The Fe-rich and Si-rich particles did not contain S and were internally mixed with other elements, including O and Ti, and could have been mixed with Al (e.g., aluminosilicates), but this could not be determined due to the background from the aluminum substrate. Particles rich in Fe and Si have been previously observed in samples from Mexico City, possibly originating from road dust and unpaved roads within the city.[83]

Ca-rich particles contained a large peak associated with Ca, and the majority of the Ca-rich particles also contained S (84 ± 3% by number) as well as C, O, Si, and Fe. While the majority of the Ca-rich particles were mixed with S, there is a small fraction (17 ± 3% by number) of Ca-rich particles present without any peaks associated with S, likely indicating there are multiple sources of Ca-rich particles in this region or different degrees of secondary processing. Particles rich in Ca may originate from natural sources such (e.g., soil resuspension from the dry Texcoco lake[84] or gypsum ($CaSO_4{\cdot}H_2O$)), as well as anthropogenic sources (e.g., coal burning, diesel combustion, cement production).[73,85]

Biological particles were classified based on the presence of a peak associated with P (> 2%), and the EDX spectra in this study were consistent with observations of biological particles from other regions, which typically contain P from phosphate,[76] as well as C originating from organic macromolecules.[46] The biological particles existed both with (71 ± 8% by number) and without (29 ± 8% by number) S, as well as with other elements including O, Na, Si, K, Ca, Ti, Cu, and/or Fe. It should be noted that limited EDX sensitivity to S (limit of detection (LOD), S > 2 mol %)[80] could mean that S is undetected by this technique in some of the particles classified, and thus the fraction of particles without S likely represents an upper bound. Overall, the results from CCSEM-EDX indicate that S is present within particles from several primary and secondary sources (carbonaceous, Ca-rich, biological), and that within these classes there is substantial particle-to-particle diversity, with some of the particles from the same general source both with and without the S.

Distribution of Sulfur across Particle Types during the Two Case Study Days. To further understand the influence of SO_2 on the presence of S within PM at the field sites during sampling, the distribution of S as measured by EDX within the different particle types was compared for the two case study days, PED and SAG, as defined above. A greater number fraction of the measured particles contained S at PED (41 ± 1% by number) than SAG (25 ± 1% by number), which is consistent with a lower SO_2 concentration at SAG leading to less particle-phase S (Figure 4). An average spectrum for each particle type with and without S is provided for the PED (Figure S6) and SAG (Figure S7) samples. For both samples, the most prevalent particle type with S was carbonaceous (Figure 4b and 4e). In PED, the vast majority of the S-containing particles (90 ± 1% by number) were carbonaceous, while for SAG fewer carbonaceous particles had S (65 ± 1% by number), likely due to lower SO_2 levels. SEM-EDX results suggest that the local SO_2 levels in Mexico City influenced particle composition and the number fraction of particles containing S at each site.

Distribution of Sulfate within Soot and Organic Aerosol. To further investigate the composition of the carbonaceous particles identified via CCSEM-EDX, single particle O-PTIR analysis, which provides information about the functional groups of chemical species through simultaneous Raman and IR microspectroscopy, was conducted on the PED and SAG samples (d_a = 0.32- 0.56 μm). The individual particles were grouped into four categories for carbonaceous particles based on their IR and Raman spectra: organic with sulfate, organic + soot with sulfate, organic without sulfate, and organic + soot without sulfate (Figure 5). Background IR and Raman spectra for the quartz substrate are provided in Figure S8. Sulfate has an anti-symmetric stretch, $\nu_{as}(SO_4)$, at ∼1100 cm^{-1} that is very IR-active and can be used to clearly identify particles as sulfate-containing with PTIR.[48] Sulfate also has a as a Raman-active (IR inactive) symmetric stretch, $\nu_s(SO_4)$, between 975-1010 cm^{-1} (depending on

https://doi.org/10.1021/acsestair.4c00048
ACS EST Air 2024, 1, 1037−1052

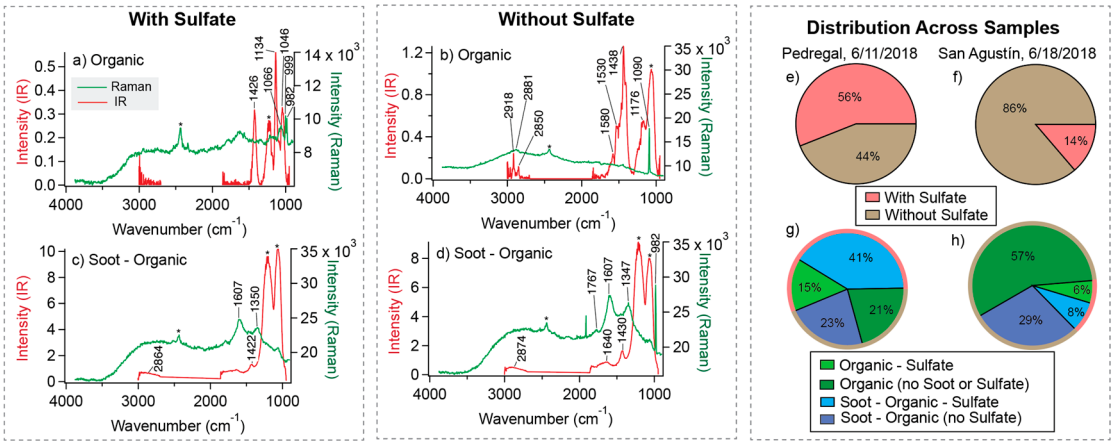

Figure 5. IR and Raman spectra of single aerosol particles (d_a = 0.32 − 0.56 μm) representative of each category are shown: (a) organic - sulfate, (b) organic (no soot or sulfate), (c) soot − organic − sulfate, and (d) soot − organic (no sulfate). Number fraction of particles with and without sulfate for the case study samples (e) PED and (f) SAG is shown. Additionally, the fraction of particles within each category (a-d) are shown for (g) PED and (h) SAG.

counterion).[48,86] With these two peaks in the complementary Raman and PTIR spectra, sulfate within individual particles can be confidently identified.

Overall, a greater number fraction of particles contained sulfate at PED (60 ± 5% by number) compared to SAG (10 ± 3% by number). The OPTIR results are overall consistent with the trend observed in particles containing S as measured by CCSEM-EDX. However, there was a greater number fraction of particles containing S measured by CCSEM-EDX for SAG (25 ±1%) compared to particles containing sulfate (10 ± 5%). It is possible that the smaller sample size (100 particles analyzed with OPTIR vs. >1000 particles with CCSEM-EDX) results in underreporting the number fraction of particles containing sulfate. Differences in the sensitivity of EDX to S vs. OPTIR to sulfate could also contribute to this discrepancy.

The Raman spectra of soot particles were separated from organic particles based on the presence of peaks near 1350 and 1610 cm^{-1} in the Raman spectra, which are the characteristic D and G bands of soot,[87−89] respectively. The D and G bands were consistent while spectra were collected, and particles did not visibly burn, indicating the bands were from soot in the sample. These particles are further classified as soot-organic due to the presence of peaks indicative of other organic species in the C−H stretching region of the IR spectra (2864 and 2874 cm^{-1}), as pure soot does not have significant signal from C−H stretching.[90] Soot particles were abundant across both case study days, representing 64 ± 5%, by number at PED and 37 ± 5%, by number at SAG of the carbonaceous particles as measured by O-PTIR (Figure 5g, h). Consistent with the CCSEM-EDX measurements and ambient SO_2 levels, more soot particles contained sulfate at PED (41 ± 5% by number) than SAG (8 ± 3% by number). This result suggests that a large fraction of the S-containing particles within the EDX-identified carbonaceous class are soot particles.

Organic particles were defined as particles with organic peaks, but without the characteristic D and G bands of soot. Representative spectra of organic particles with and without a sulfate peak are shown in Figure 5a and 5b, respectively. Additionally, 21 ± 4%, by number, of the organic particles had Raman spectra saturated with fluorescence, which could indicate that the organic species contain aromatic functional groups. The number fraction of organic particles with and without sulfate was compared for the two case study days, and, similar to the soot particles, the number fraction of organic particles with sulfate was greater for the PED sample (15 ± 4% by number) than for the SAG sample (6 ± 2% by number).

A benefit of vibrational spectroscopy is that sulfate (1100 cm^{-1}), bisulfate (1040 cm^{-1}), and organosulfates (~1070 cm^{-1}) can be clearly distinguished from each other. Notably, a peak (1066 cm^{-1})[52,91] present in the organic particle with sulfate spectra (Figure 5a) is associated with the presence of particulate organosulfates, which includes MTS. Organosulfates are formed within SOA, indicating that these particles are secondary and mostly mixtures of sulfate, SOA, and organosulfates. Having identified the presence of organosulfates using single-particle characterization methods, it is important to determine their concentration and potentially their sources (e.g., isoprene), which was investigated with HILIC/ESI-HR-QTOFMS.

Quantification of MTS and MT. The molecular speciation of organosulfates can determine the VOC precursor from which the SOA formed, and isoprene-derived MTSs, including both 2-MTS and 3-MTS, were quantified within $PM_{2.5}$ from Mexico City. MTS forms from the acid-driven reactive uptake of IEPOX (formed under low-NO conditions) and subsequent nucleophilic attack by sulfate within particles (Figure 6a).[92] The $PM_{2.5}$ mass concentration of MTS measured by HILIC/(−)ESI-HR-QTOFMS across measurement sites and sampling days ranged from below the LOQ up to 145 ng/m^3 (Figure 6b). The mass concentrations of MTS were greater for all sampling days at the Pedregal site (avg. 80 ng/m^3, range 20−150 ng/m^3) in comparison to the San Agustín site (avg. 20 ng/m^3; range below LOQ − 40 ng/m^3), consistent with the greater levels of SO_2 at Pedregal. In addition to MTS, we quantified the formation of another key IEPOX reaction product, MT, that forms from the reactive uptake of IEPOX followed by nucleophilic attack by water.[93] MT was observed on all of the sampling days at both sites. Similar to MTS, the particulate mass concentration of MT was overall greater at the Pedregal site (avg. 110 ng/m^3; range 60−190 ng/m^3) than at the San Agustín site (avg. 40 ng/m^3; range 8−60 ng/m^3). This could indicate that SO_2 levels increase the formation of other non-sulfated iSOA compounds, perhaps by lowering the pH of the particles, which increases acid-driven IEPOX reactions.[94,95]

https://doi.org/10.1021/acsestair.4c00048
ACS EST Air 2024, 1, 1037−1052

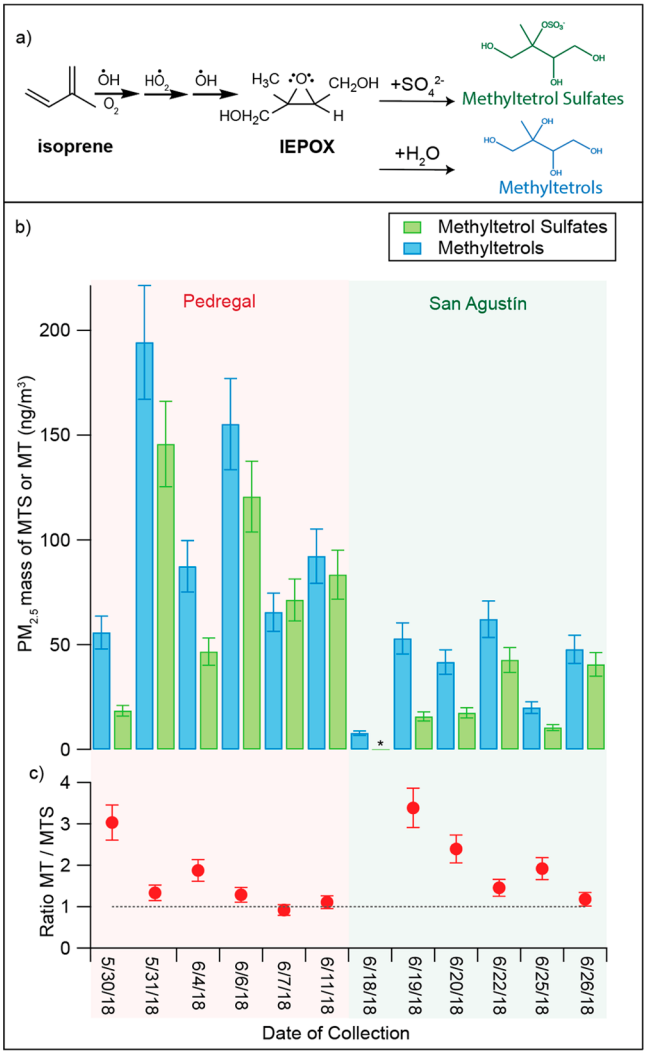

Figure 6. (a) Overview of mechanism of formation of methyltetrol sulfates and methyltetrols.[101] (b) Mass concentrations of methyltetrol sulfates (MTS, green) and methyltetrols (MT, blue) quantified in samples from Pedregal and San Agustín. Error bars represent% relative standard error in HILIC/ESI-HR-QTOFMS analysis (14%). Asterisks indicates that quantification is below the LOQ. (c) Ratio of mass of MT to the mass of MTS. Error bars represent% relative standard error. Dotted line denotes to a 1:1 ratio of MT to MTS products for reference.

The mass ratio of MT to MTS (MT:MTS) was calculated and compared between the samples (Figure 6c). For all sampling days, the mass of MT was equal to or greater than the mass of MTS. The highest MT:MTS ratios occurred on 5/30/18 at the Pedregal location (3.0) and 6/19/18 at the San Agustín location (3.4), suggesting a greater amount of particle-phase water (i.e., the nucleophile required for the formation of MT products) or lower amounts of sulfate. It should be noted that during transport and storage, it is possible that degradation of MTS occurred on the filter samples before analysis through the slow hydrolysis of MTS to MT, as has been previously observed.[59] This would result in an overestimation of the mass concentration of MT compared to MTS, which could result in a higher MT:MTS ratio observed for all samples.

The mass concentrations of MTS and MT products in this study were compared to other field sites in which these species have been quantified globally to place the measurements in Mexico City within a global context (Table 1). In this study, the mass concentration of MTS ranged from below the LOQ to 150 ng/m^3. In a recent study conducted by Zhang et al.,[33] MTS isomers were quantified throughout a year-long period in three large urban cities in China: Beijing, Hefei, and Kunming. The mass concentration range of both MTS and MT compounds quantified in this present study in Mexico City were greater than what was measured in all three urban sites in China.[33] Additionally, MTS were recently quantified in Delhi, India, during the pre-monsoon (early summer) and post-monsoon (fall) season,[34] and the concentration of MTS measured in this study in Mexico City was also greater than those measured in Delhi. These results indicate that Mexico City could have a larger contribution of low-NO iSOA to total SOA aerosol mass compared to many other urban megacities globally. This could be due to high SO_2 emissions in Mexico City, resulting in the prevalence of acidic sulfate particles onto which reactive uptake of IEPOX can occur.

Despite concentrations of MTS and MT measured in Mexico City in this study being greater than the other megacities where they have been quantified, the concentrations of these species were less than those previously measured in many isoprene-rich rural and urban environments (Table 1). The mass concentration of MTS was previously quantified in two rural regions including Look Rock, Tennessee, and Manaus, Brazil, reporting 2,334 ng/m^3 and 390 ng/m^3, respectively.[28] In these rural regions, the mass concentration of MTS was much greater than that identified in Mexico City in this study, which is attributable to the higher local isoprene concentrations. A significantly larger mass concentration of MTS was measured in Atlanta, Georgia, which is due to the city's proximity to isoprene-rich forested regions, as previously established.[97]

Interestingly, the different mass concentrations of MTS between this study and other studies listed above seems to suggest a different trend for MTS than for MT (Table 1). Similar to MTS, a greater mass concentration of MT, 861 ng/m^3, was quantified at Look Rock, Tennessee[28] than in this study. However, despite a greater concentration of MTS, MT quantified at Manaus, Brazil, was less than the maximum observed in this study (Mexico City),[28] which could indicate that aerosol properties in addition to isoprene emissions help determine the production of MT. A greater mass concentration of MTS than MT was observed at both rural sites by Cui et al.,[59] whereas the mass concentration of MT exceeded that of MTS for the majority of the Mexico City field samples in this study. It is possible that the sampling conditions (e.g., hydrolysis of MTS to MT) could have resulted in an overestimation of MT in these samples. It is also possible that meteorological conditions (e.g., isoprene flux or SO_2) or aerosol properties (e.g., particle pH or liquid water content) could influence the ratio of these products formed and result in an enhanced formation of MT products on certain days.

For all sampling days at both field sites the air mass remained within the Mexico City basin (Figure S9–S20), indicating that the isoprene source is likely local, such as vegetation within Mexico City from net-leaf oak trees as estimated by Dominguez-Taylor et al.[45] or anthropogenic sources (e.g., traffic emissions) discussed by Hodzic et al.[99] Estimates from the Models of Emissions from Gases and Aerosols from Nature (MEGAN) model and GEOS-CHEM global modeling indicate that isoprene emissions in Mexico

https://doi.org/10.1021/acsestair.4c00048
ACS EST Air 2024, 1, 1037−1052

Table 1. Mass Concentrations of Methyltetrol Sulfates and Methyltetrols from Field Observations Globally, with a Focus on Urban Measurements[a]

Location	Classification	Season	MTS (ng/m^3)	MT (ng/m^3)	Reference
Mexico City, Mexico	Urban	Summer	below LOQ (0.2 ng/m^3) − 150	8−190	This study
Beijing, China	Urban	Year-round	0.13−1.41	0.26−43.2	33
Hefei, China	Urban	Year-round	0.18−4.12	0.59−88.5	33
Kunming, China	Urban	Year-round	4.83−84.6	0.15−3.32	33
Delhi, India	Urban	Summer and Fall	17.91−38.79	N/A	34
Athens, Greece	Urban	Year-round	2.5−133	N/A	96
Patra, Greece	Urban	Year-round	6.1−281	N/A	96
Atlanta, Georgia, United States	Urban	Summer	419−4763	N/A	97
Cape Grim, Australia	Marine	Winter and Summer	n.d. (LOD=1.72 μg/L)	n.d. (LOD = 7.74 μg/L) − 4.21	59
Look Rock, Tennessee, United States	Rural	Summer	2334	861	28
Manaus, Brazil	Rural	Summer	390	137	28
Zion, Illinois	Rural	Summer	0.4−832.8	0.1−28.3	98

[a]Columns indicate location of sampling, classification of location, season of sampling, mass concentration of methyltetrol sulfates, mass concentration of methyltetrols, and reference of study. n.d. indicates that measurement in the study did not detect product.

City could be greater than emissions in other urban megacities investigated previously.[100] Results from a GEOS-Chem global model simulation from July 2013 − June 2014 also predicted a significant surface concentration of IEPOX-SOA.[101] Further research is needed to characterize the formation of low-NO iSOA in megacities without large isoprene sources (e.g., Atlanta) to better understand how vegetation influences iSOA in urban regions.

To further investigate the abundance of iSOA in Mexico City, especially S-containing iSOA products, filter extracts were analyzed for the presence of additional iSOA compounds. An example of the extracted ion chromatogram for each compound is shown from PED (Figure 7). The ambient concentration of NO influences the oxidation pathway that isoprene undergoes to form SOA.[70,102−104] Given the complexities associated with the terms "low-NO_x" and "high-NO_x" as discussed by Wennberg et al.,[105] we have chosen to refer to these regimes as low-NO and high-NO conditions. While there isn't an explicit range for ambient low-NO conditions, in chamber experiments, low-NO conditions have been represented with a NO mixing ratio of <1 ppb.[25,106] From isoprene oxidation, low-NO conditions allow for RO2 radicals to predominantly react with hydroperoxyl radicals (HO2), eventually yielding IEPOX that forms SOA under these conditions.[103,107] Interestingly, iSOA products from both the low-NO (Figure 7a-d) and high-NO (Figure 7e-h) reaction pathways were observed in these samples, indicating that during sampling conditions, ambient NO levels could have led to both reaction pathways occurring. This was also observed by Zhang et al.[33] in their study of three major urban cities in China (Hefei, Beijing, and Kunming), suggesting that products from these two pathways may co-exist in urban regions where NO levels fluctuate throughout the day. During sampling conditions in this study, the ambient NO levels varied widely; the diel variation ranged from Δ9 ppb to Δ87 ppb at Pedregal and from Δ16 ppb to Δ79 ppb at San Agustín. It is possible that, as NO levels fluctuate within a 24-h period, the iSOA product formation in the region could subsequently fluctuate between the high-NO and low-NO reaction pathways. In addition to the results from PED shown in Figure 7, all of the filter samples from the sampling days at both sites were analyzed for the presence of these eight species, and all were identified in the filter samples from all sampling days at the Pedregal and San Agustín field sites. Their relative abundance across sampling days and locations is plotted in Figure S21. Unfortunately, due to a lack of standards for these compounds, their atmospheric concentrations could not be quantified. These results further demonstrate the importance of iSOA in the densely populated urban environment of Mexico City, Mexico, and suggest that there could be an abundance of iSOA products in this region. More so, a diversity of iSOA species were observed, including products from both the low-NO and high-NO regime, suggesting that these products could co-exist in urban environments as NO levels fluctuate.

Comparison of Environmental Conditions During Sampling Days. Given that the measurements were not conducted simultaneously at the two sites, differences in the mass concentrations of the species and MT:MTS product ratios between the two sites could also be due to differences in meteorological conditions and emissions across sampling days. To investigate whether the difference in iSOA product mass at the Pedregal and San Agustín sites could be connected to meteorology, the temperature and relative humidity (RH) measured by the RAMA monitoring station during the sampling periods were compared for the case study days (Figure S2) as well as at the San Agustín and Pedregal locations across the entire sampling period (Figure S3 and S4). The Pedregal site experienced higher temperatures during the sampling period (5/30/2018 to 6/11/2018), with the 24-h daily average ranging from 20 to 24 °C. In comparison, the San Agustín site experienced lower temperatures during the sampling period (6/18/2018 to 6/26/2018), ranging from 17 to 20 °C. Higher ambient temperatures increase the isoprene emission flux,[108] which could result in higher iSOA product formation with higher temperatures at Pedregal. To investigate whether the ambient temperature correlates with iSOA formation, the sum of the mass concentrations of MTS and MT was compared to the average temperature during the 24-h sampling periods. However, no clear trend was observed between temperature and MTS and MT mass concentrations (Figure S22). Given the relatively small temperature difference, it remains unclear whether temperature was an influencing factor for the differences in iSOA formation.

A greater ambient RH results in an increase in aerosol liquid water content, which dilutes aerosol particles and results in a decrease in aerosol acidity.[109] The formation of MTS and MT are both enhanced under acidic conditions,[26] which means that the formation of these species could decrease as RH increases.

https://doi.org/10.1021/acsestair.4c00048
ACS EST Air 2024, 1, 1037−1052

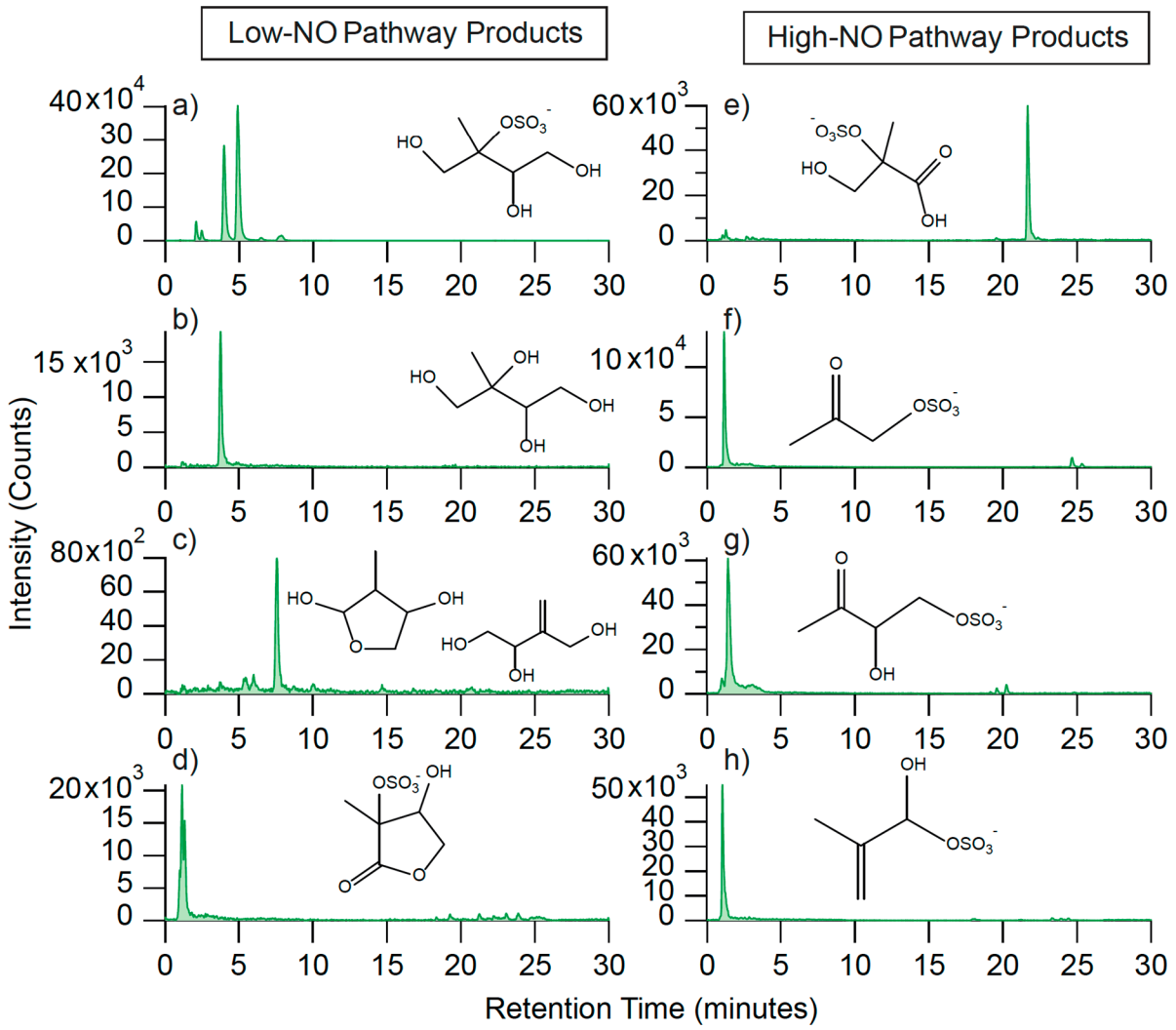

Figure 7. HILIC/(−)ESI-HR-QTOFMS extracted ion chromatograms (EICs) collected from Pedregal 6/11/2018 sample. Includes the deprotonated molecules corresponding to (a) methyltetrol sulfates (MTS), $C_5H_{11}O_7S^-$, at m/z 215.023, (b) methyltetrols (MT), $C_5H_{11}O_4^-$, at m/z 135.066, (c) C_5-alkene triols, $C_5H_9O_3^-$, at m/z 117.055, (d) isoprene-organosulfate oxidation product, $C_5H_7O_7S^-$, at m/z 210.991, (e) 2-methyl glyceric acid, $C_4H_7O_7S^-$, at m/z 198.991, (f) hydroxyacetone sulfate, $C_3H_5O_5S^-$, at m/z 152.986, (g) isoprene-organosulfate, $C_4H_7O_6S^-$, at m/z 182.996, and (h) isoprene-organosulfate, $C_4H_7O_5S$, at m/z 167.001.

To investigate whether the ambient RH correlates with iSOA formation, the average RH during the 24-h sampling period was also compared to the sum of the mass concentration of MTS and MT species (Figure S22). Similar to the ambient temperature, no clear trend was observed, and the difference in MTS and MT mass concentration cannot be solely attributed to the differences in ambient temperature and RH.

Conclusions and Atmospheric Implications. This study investigates the distribution of sulfur within a population of aerosol particles, the presence of organosulfates, and concentrations of iSOA at two field sites in Mexico City, Mexico. To better understand the speciation of S-containing compounds within the aerosol particles, the chemical composition of individual aerosol particles within a subset of $PM_{2.5}$ is analyzed for the distribution of S across particle types. Additionally, filter samples were analyzed for the formation of key organosulfate and non-sulfated organic species formed from the reactive uptake of the isoprene oxidation product IEPOX to sulfate particles. Through individual particle analysis, five different classes of aerosol particles were observed: carbonaceous, Ca-rich, Si-Rich, Fe-rich, and biological. Within these classes, the greatest number fraction of particles containing S were carbonaceous particles. Complementary O-PTIR and Raman microspectroscopy of single aerosol particles revealed that these carbonaceous particles are a mix of soot and organic aerosol, and that the organic aerosol particles contain a peak corresponding to organosulfates. Through filter analysis, a significant mass of MTS and MT, which form through the low-NO pathway, were quantified. In addition, several iSOA products from both the low-NO and high-NO reaction pathways were observed. Notably, a greater mass of MTS and MT products were quantified at these Mexico City field sites compared to other megacities globally. Given that previous research did not identify iSOA as a significant class of PM in Mexico City,[42,44] our results indicate that it is possible that emission sources influencing the formation of iSOA may have changed since previous measurements campaigns and that iSOA could contribute more significantly to PM within Mexico City than previously thought. Additionally, our results indicate that sulfur is not evenly distributed across the aerosol population, with some classes of aerosol particles existing without any sulfur. It is

https://doi.org/10.1021/acsestair.4c00048
ACS EST Air 2024, 1, 1037−1052

possible that the mixing state of sulfur in other urban locations could be analogous, and future studies should characterize the mixing state of aerosol populations in urban environments.

As the number fraction of individuals living in megacities globally increases, understanding the chemistry of air pollution in these environments becomes increasingly important. Mexico City is the largest city in North America and its metropolitan area is home to over 20 million people. The combination of its topographical geography as well as high emissions from a number of sources (i.e., industrial, vehicular, biomass burning, resuspended dust, etc.) result in persistent poor air quality in the city.[110,111] SO_2 emissions are a significant source of pollution in Mexico City. While there have been significant reductions in SO_2 in Mexico City since the early 2000's,[57] emissions have remained high over the past decade (Figure S23). Our results indicate that sulfur-containing particles are still a significant component of PM within Mexico City impacting SOA formation (i.e., iSOA) in this region, which may be underrepresented in measurements quantifying sulfate in PM due to the conversion of some sulfate to organosulfur species. Thus, future air quality initiatives focused on further SO_2 emission reductions are likely to lead to even greater reductions in SOA formation in the region. Additionally, since the 2006 MILAGRO campaign, initiatives have been developed to increase green spaces within the city,[112] which could inadvertently increase biogenic VOC emissions such as isoprene. Similar greening efforts have been projected to increase SOA formation from increased emission of the biogenic VOC precursors in Los Angeles basin.[113] Future air quality initiatives could consider increasing the type and density of vegetation in Mexico City with a lower secondary organic aerosol formation potential (SOAP).[113] To guide these initiatives, future work should characterize the density of isoprene-emitting vegetation within Mexico City and investigate their influence on SOA formation. Our study expands understanding of the sources and composition of S-containing aerosol particles in Mexico City, specifically improving understanding of iSOA by quantifying the mass of key products. The chemical composition of aerosol particles is known to impact their resulting health effects after exposure, and iSOA has well-established chronic negative health effects, such as inducing oxidative stress in the pulmonary system.[30,31] The improved understanding of sulfate and organosulfates from this study can help efforts aimed at mitigating the harmful effects of atmospheric aerosol pollution in Mexico City and in other urban megacities globally.

■ ASSOCIATED CONTENT

Supporting Information

The Supporting Information is available free of charge at https://pubs.acs.org/doi/10.1021/acsestair.4c00048.

Additional information including a table with details of field sample collection (Table S1); concentration of NOx (NO + NO2) at field sites (Figure S1); environmental conditions at field sites (Figures S2−S4); graphic describing the categorization of aerosol samples as determined by CCSEM EDX (Figure S5); average EDX spectra for PED particle types (Figure S6); average spectra for SAG particle types (Figure S7); background O-PTIR and Raman spectra (Figure S8); HYSPLIT analysis during field collection (Figures S9−S20); relative abundance of iSOA products across sampling days (Figure S21); comparison of environmental conditions; comparison of environmental conditions to MTS and MT abundance (Figure S22); and concentration of SO_2 at field sites from 2013−2023 (Figure S23) (PDF)

■ AUTHOR INFORMATION

Corresponding Author

Andrew P. Ault − *Department of Chemistry, University of Michigan, Ann Arbor, Michigan 48109, United States;* orcid.org/0000-0002-7313-8559; Email: aulta@umich.edu

Authors

Madeline E. Cooke − *Department of Chemistry, University of Michigan, Ann Arbor, Michigan 48109, United States*

Cara M. Waters − *Department of Chemistry, University of Michigan, Ann Arbor, Michigan 48109, United States*

Joel Y. Asare − *Department of Chemistry, University of Michigan, Ann Arbor, Michigan 48109, United States*

Jessica A. Mirrielees − *Department of Chemistry, University of Michigan, Ann Arbor, Michigan 48109, United States*

Andrew L. Holen − *Department of Chemistry, University of Michigan, Ann Arbor, Michigan 48109, United States;* orcid.org/0009-0006-7654-2019

Molly P. Frauenheim − *Department of Environmental Sciences and Engineering, Gillings School of Global Public Health, University of North Carolina at Chapel Hill, Chapel Hill, North Carolina 27599, United States*

Zhenfa Zhang − *Department of Environmental Sciences and Engineering, Gillings School of Global Public Health, University of North Carolina at Chapel Hill, Chapel Hill, North Carolina 27599, United States*

Avram Gold − *Department of Environmental Sciences and Engineering, Gillings School of Global Public Health, University of North Carolina at Chapel Hill, Chapel Hill, North Carolina 27599, United States;* orcid.org/0000-0003-1383-6635

Kerri A. Pratt − *Department of Chemistry, University of Michigan, Ann Arbor, Michigan 48109, United States; Department of Earth and Environmental Sciences, University of Michigan, Ann Arbor, Michigan 48109, United States;* orcid.org/0000-0003-4707-2290

Jason D. Surratt − *Department of Environmental Sciences and Engineering, Gillings School of Global Public Health, University of North Carolina at Chapel Hill, Chapel Hill, North Carolina 27599, United States; Department of Chemistry, College of Arts and Sciences, University of North Carolina at Chapel Hill, Chapel Hill, North Carolina 27599, United States;* orcid.org/0000-0002-6833-1450

Luis A. Ladino − *Instituto de Ciencias de la Atmósfera y Cambio Climático, Universidad Nacional Autónoma de México (UNAM), México City, México 04510*

Complete contact information is available at: https://pubs.acs.org/10.1021/acsestair.4c00048

Funding

This work was supported by the National Science Foundation (NSF) under Grants AGS-1703019 and AGS-2040610 (Ault), as well as AGS-1703535 and AGS-2039788 (Surratt). The University of Michigan Department of Chemistry provided additional support. M.E.C. was supported by an NSF Graduate

Research Fellowship (NSF-GRFP) DGE-1841052. C.W.M. was supported by an NSF-GRFP (DGE-2241144). J.Y.A. was supported through the NSF Research Experience for Undergraduates (REU) program in the Department of Chemistry at the University of Michigan (Grant CHE-1950066). A portion of this research was performed on a project award 60327 from the Environmental Molecular Sciences Laboratory, a DOE Office of Science User Facility sponsored by the Biological and Environmental Research program under Contract No. DE-AC05-76RL01830.

Notes

The authors declare no competing financial interest.

■ ACKNOWLEDGMENTS

This paper is submitted in memory of Anel Alfonso, our collaborator and friend, who assisted in instrument deployment and sampling. We gratefully acknowledge Anel Alfonso, Harry Alvarez, Giovanni Carabali, and Ma. Isabel Saavedra for their support during the sampling, as well as the RAMA for allowing us to deploy our instruments to their monitoring sites and providing the data included in Figure 2 and Figures S1−S4 and S22−S23. CCSEM-EDX analyses were performed at the Environmental Molecular Sciences Laboratory (EMSL), a national scientific user facility located at the Pacific Northwest National Laboratory (PNNL) and sponsored by the Office of Biological and Environmental Research of the U.S. Department of Energy. Additional SEM-EDX analysis was conducted at the Michigan Center for Materials Characterization (MC^2), and the authors would like to acknowledge the University of Michigan College of Engineering for financial support including partially subsidizing the use of electron microscopy instrumentation and staff assistance. The authors gratefully acknowledge the NOAA Air Resources Laboratory (ARL) for the provision of the HYSPLIT transport and dispersion model and/or READY website (https://www.ready.noaa.gov) used in this publication. We acknowledge the use of imagery from the Worldview Snapshots application (https://wvs.earthdata.nasa.gov), part of the Earth Observing System Data and Information System (EOSDIS). Satellite imagery for Figure 1b courtesy of Earthstar Geographics LLC.

■ REFERENCES

(1) Carabali, G.; Villanueva-Macias, J.; Ladino, L. A.; Álvarez-Ospina, H.; Raga, G. B.; Andraca-Ayala, G.; Miranda, J.; Grutter, M.; Silva, M. M.; Riveros-Rosas, D. Characterization of aerosol particles during a high pollution episode over Mexico City. *Sci. Rep.* **2021**, *11* (1), 22533.

(2) Bravo Alvarez, H.; Sosa Echeverria, R.; Sanchez Alvarez, P.; Krupa, S. Air Quality Standards for Particulate Matter (PM) at high altitude cities. *Environ. Pollut* **2013**, *173*, 255−6.

(3) Molina, L. T.; Kolb, C. E.; De Foy, B.; Lamb, B. K.; Brune, W. H.; Jimenez, J. L.; Ramos-Villegas, R.; Sarmiento, J.; Paramo-Figueroa, V. H.; Cardenas, B.; Gutierrez-Avedoy, V.; Molina, M. J. Air quality in North America's most populous city - overview of the MCMA-2003 campaign. *Atmos. Chem. and Phys.* **2007**, *7* (10), 2447−2473.

(4) Jimenez, J. L.; Donahue, A. S. H.; Prevot, Q.; Zhang, J. H.; Kroll, P. F.; DeCarlo, J. D.; Allan, H.; Coe, N. L.; Ng, A. C.; Aiken, K. S.; Docherty, I. M.; Ulbrich, A. P.; Grieshop, A. L.; Robinson, J.; Duplissy, J. D.; Smith, K. R.; Wilson, V. A.; Lanz, C.; Hueglin, Y. L.; Sun, J.; Tian, A.; Laaksonen, T.; Raatikainen, J.; Rautiainen, P.; Vaattovaara, M.; Ehn, M.; Kulmala, J. M.; Tomlinson, D. R.; Collins, M. J.; Cubison, E.; et al. Evolution of Organic Aerosols in the Atmosphere. *Science* **2009**, *326*, 1525−1529.

(5) Chen, Y.; Dombek, T.; Hand, J.; Zhang, Z.; Gold, A.; Ault, A. P.; Levine, K. E.; Surratt, J. D. Seasonal Contribution of Isoprene-Derived Organosulfates to Total Water-Soluble Fine Particulate Organic Sulfur in the United States. *ACS Earth Space Chem.* **2021**, *5* (9), 2419−2432.

(6) Seinfeld, J. H.; Pandis, S. N. *Atmospheric chemistry and physics: From air pollution to climate change*, 3rd ed.; John Wiley & Sons.: 2016.

(7) Hegg, D. A. The importance of liquid phase oxidation of SO2 in the troposphere. *J. Geophys. Res: Atmos.* **1985**, *90* (D2), 3773−3779.

(8) Hand, J. L.; Schichtel, B. A.; Malm, W. C.; Pitchford, M. L. Particulate sulfate ion concentration and SO2 emission trends in the United States from the early 1990s through 2010. *Atmos. Chem. Phys.* **2012**, *12* (21), 10353−10365.

(9) Kanakidou, M.; Seinfeld, J. H.; Pandis, S. N.; Barnes, I.; Dentener, F. J.; Facchini, M. C.; Van Dingenen, R.; Ervens, B.; Nenes, A.; Nielsen, C. J.; Swietlicki, E.; Putaud, J. P.; Balkanski, Y.; Fuzzi, S.; Horth, J.; Moortgat, G. K.; Winterhalter, R.; Myhre, C. E. L.; Tsigaridis, K.; Vignati, E.; Stephanou, E. G.; Wilson, J. Organic aerosol and global climate modelling: a review. *Atmos. Chem. Phys.* **2005**, *5* (4), 1053−1123.

(10) Saxena, P.; Hildemann, L. M. Water-soluble organics in atmospheric particles: A critical review of the literature and application of thermodynamics to identify candidate compounds. *J. Atmos. Chem.* **1996**, *24* (1), 57−109.

(11) Putaud, J. P.; Van Dingenen, R.; Alastuey, A.; Bauer, H.; Birmili, W.; Cyrys, J.; Flentje, H.; Fuzzi, S.; Gehrig, R.; Hansson, H. C.; Harrison, R. M.; Herrmann, H.; Hitzenberger, R.; Hüglin, C.; Jones, A. M.; Kasper-Giebl, A.; Kiss, G.; Kousa, A.; Kuhlbusch, T. A. J.; Löschau, G.; Maenhaut, W.; Molnar, A.; Moreno, T.; Pekkanen, J.; Perrino, C.; Pitz, M.; Puxbaum, H.; Querol, X.; Rodriguez, S.; Salma, I.; Schwarz, J.; Smolik, J.; Schneider, J.; Spindler, G.; ten Brink, H.; Tursic, J.; Viana, M.; Wiedensohler, A.; Raes, F. A European aerosol phenomenology - 3: Physical and chemical characteristics of particulate matter from 60 rural, urban, and kerbside sites across Europe. *Atmos. Environ.* **2010**, *44* (10), 1308−1320.

(12) Aiken, A. C.; De Foy, B.; Wiedinmyer, C.; Decarlo, P. F.; Ulbrich, I. M.; Wehrli, M. N.; Szidat, S.; Prevot, A. S. H.; Noda, J.; Wacker, L.; Volkamer, R.; Fortner, E.; Wang, J.; Laskin, A.; Shutthanandan, V.; Zheng, J.; Zhang, R.; Paredes-Miranda, G.; Arnott, W. P.; Molina, L. T.; Sosa, G.; Querol, X.; Jimenez, J. L. Mexico city aerosol analysis during MILAGRO using high resolution aerosol mass spectrometry at the urban supersite (T0) - Part 2: Analysis of the biomass burning contribution and the non-fossil carbon fraction. *Atmos. Chem. Phys.* **2010**, *10* (12), 5315−5341.

(13) Aiken, A. C.; Salcedo, D.; Cubison, M. J.; Huffman, J. A.; Decarlo, P. F.; Ulbrich, I. M.; Docherty, K. S.; Sueper, D.; Kimmel, J. R.; Worsnop, D. R.; Trimborn, A.; Northway, M.; Stone, E. A.; Schauer, J. J.; Volkamer, R. M.; Fortner, E.; De Foy, B.; Wang, J.; Laskin, A.; Shutthanandan, V.; Zheng, J.; Zhang, R.; Gaffney, J.; Marley, N. A.; Paredes-Miranda, G.; Arnott, W. P.; Molina, L. T.; Sosa, G.; Jimenez, J. L. Mexico City aerosol analysis during MILAGRO using high resolution aerosol mass spectrometry at the urban supersite (T0) - Part 1: Fine particle composition and organic source apportionment. *Atmos. Chem. Phys.* **2009**, *9* (17), 6633−6653.

(14) Molina, L. T.; Madronich, S.; Gaffney, J. S.; Apel, E.; De Foy, B.; Fast, J.; Ferrare, R.; Herndon, S.; Jimenez, J. L.; Lamb, B.; Osornio-Vargas, A. R.; Russell, P.; Schauer, J. J.; Stevens, P. S.; Volkamer, R.; Zavala, M. An overview of the MILAGRO 2006 Campaign: Mexico City emissions and their transport and transformation. *Atmos. Chem. Phys.* **2010**, *10* (18), 8697−8760.

(15) Moffet, R. C.; Henn, T. R.; Tivanski, A. V.; Hopkins, R. J.; Desyaterik, Y.; Kilcoyne, A. L. D.; Tyliszczak, T.; Fast, J.; Barnard, J.; Shutthanandan, V.; Cliff, S. S.; Perry, K. D.; Laskin, A.; Gilles, M. K. Microscopic characterization of carbonaceous aerosol particle aging in the outflow from Mexico City. *Atmos. Chem. Phys.* **2010**, *10* (3), 961−976.

(16) Moffet, R. C.; Desyaterik, Y.; Hopkins, R. J.; Tivanski, A. V.; Gilles, M. K.; Wang, Y.; Shutthanandan, V.; Molina, L. T.; Abraham,

https://doi.org/10.1021/acsestair.4c00048
ACS EST Air 2024, 1, 1037−1052

R. G.; Johnson, K. S.; Mugica, V.; Molina, M. J.; Laskin, A.; Prather, K. A. Characterization of aerosols containing Zn, Pb, and Cl from an industrial region of Mexico City. *Environ. Sci. Technol.* **2008**, *42* (19), 7091−7097.
(17) Moffet, R. C.; de Foy, B.; Molina, L. T.; Molina, M. J.; Prather, K. A. Measurement of ambient aerosols in northern Mexico City by single particle mass spectrometry. *Atmos. Chem. Phys.* **2008**, *8* (16), 4499−4516.
(18) Querol, X.; Pey, J.; Minguillón, M. C.; Pérez, N.; Alastuey, A.; Viana, M.; Moreno, T.; Bernabé, R. M.; Blanco, S.; Cárdenas, B.; Vega, E.; Sosa, G.; Escalona, S.; Ruiz, H.; Artíñano, B. PM speciation and sources in Mexico during the MILAGRO-2006 Campaign. *Atmos. Chem. Phys.* **2008**, *8* (1), 111−128.
(19) Stone, E. A.; Snyder, D. C.; Sheesley, R. J.; Sullivan, A. P.; Weber, R. J.; Schauer, J. J. Source apportionment of fine organic aerosol in Mexico City during the MILAGRO experiment 2006. *Atmos. Chem. Phys.* **2008**, *8*, 1249−1259.
(20) Brüggemann, M.; Xu, R.; Tilgner, A.; Kwong, K. C.; Mutzel, A.; Poon, H. Y.; Otto, T.; Schaefer, T.; Poulain, L.; Chan, M. N.; Herrmann, H. Organosulfates in Ambient Aerosol: State of Knowledge and Future Research Directions on Formation, Abundance, Fate, and Importance. *Environ. Sci. Technol.* **2020**, *54* (7), 3767−3782.
(21) Guenther, A.; Karl, T.; Harley, P.; Wiedinmyer, C.; Palmer, P. I.; Geron, C. Estimates of global terrestrial isoprene emissions using MEGAN (Model of Emissions of Gases and Aerosols from Nature). *Atmos. Chem. Phys.* **2006**, *6* (11), 3181−3210.
(22) Froyd, K. D.; Murphy, S. M.; Murphy, D. M.; de Gouw, J. A.; Eddingsaas, N. C.; Wennberg, P. O. Contribution of isoprene-derived organosulfates to free tropospheric aerosol mass. *Proc. Natl. Acad. Sci. U. S. A.* **2010**, *107* (50), 21360−5.
(23) Bates, K. H.; Crounse, J. D.; St. Clair, J. M.; Bennett, N. B.; Nguyen, T. B.; Seinfeld, J. H.; Stoltz, B. M.; Wennberg, P. O. Gas Phase Production and Loss of Isoprene Epoxydiols. *J. Phys. Chem. A* **2014**, *118* (7), 1237−1246.
(24) Wennberg, P. O.; Bates, K. H.; Crounse, J. D.; Dodson, L. G.; McVay, R. C.; Mertens, L. A.; Nguyen, T. B.; Praske, E.; Schwantes, R. H.; Smarte, M. D.; St Clair, J. M.; Teng, A. P.; Zhang, X.; Seinfeld, J. H. Gas-Phase Reactions of Isoprene and Its Major Oxidation Products. *Chem. Rev.* **2018**, *118* (7), 3337−3390.
(25) Surratt, J. D.; Murphy, S. M.; Kroll, J. H.; Ng, N. L.; Hildebrandt, L.; Sorooshian, A.; Szmigielski, R.; Vermeylen, R.; Maenhaut, W.; Claeys, M.; Flagan, R. C.; Seinfeld, J. H. Chemical Composition of Secondary Organic Aerosol Formed from the Photooxidation of Isoprene. *J. Phys. Chem. A* **2006**, *110* (31), 9665−9690.
(26) Surratt, J. D.; Lewandowski, M.; Offenberg, J. H.; Jaoui, M.; Kleindienst, T. E.; Edney, E. O.; Seinfeld, J. H. Effect of Acidity on Secondary Organic Aerosol Formation from Isoprene. *Environ. Sci. Technol.* **2007**, *41* (15), 5363−5369.
(27) Surratt, J. D.; Kroll, J. H.; Kleindienst, T. E.; Edney, E. O.; Claeys, M.; Sorooshian, A.; Ng, N. L.; Offenberg, J. H.; Lewandowski, M.; Jaoui, M.; Flagan, R. C.; Seinfeld, J. H. Evidence for Organosulfates in Secondary Organic Aerosol. *Environ. Sci. Technol.* **2007**, *41* (2), 517−527.
(28) Cui, T.; Zeng, Z.; dos Santos, E. O.; Zhang, Z.; Chen, Y.; Zhang, Y.; Rose, C. A.; Budisulistiorini, S. H.; Collins, L. B.; Bodnar, W. M.; de Souza, R. A. F.; Martin, S. T.; Machado, C. M. D.; Turpin, B. J.; Gold, A.; Ault, A. P.; Surratt, J. D. Development of a hydrophilic interaction liquid chromatography (HILIC) method for the chemical characterization of water-soluble isoprene epoxydiol (IEPOX)-derived secondary organic aerosol. *Environ. Sci.: Processes Impacts* **2018**, *20* (11), 1524−1536.
(29) Fang, T.; Huang, Y.-K.; Wei, J.; Monterrosa Mena, J. E.; Lakey, P. S. J.; Kleinman, M. T.; Digman, M. A.; Shiraiwa, M. Superoxide Release by Macrophages through NADPH Oxidase Activation Dominating Chemistry by Isoprene Secondary Organic Aerosols and Quinones to Cause Oxidative Damage on Membranes. *Environ. Sci. Technol.* **2022**, *56* (23), 17029−17038.
(30) Eaves, L. A.; Smeester, L.; Hartwell, H. J.; Lin, Y.-H.; Arashiro, M.; Zhang, Z.; Gold, A.; Surratt, J. D.; Fry, R. C. Isoprene-Derived Secondary Organic Aerosol Induces the Expression of MicroRNAs Associated with Inflammatory/Oxidative Stress Response in Lung Cells. *Chem. Res. Toxicol.* **2020**, *33* (2), 381−387.
(31) Lin, Y.-H.; Arashiro, M.; Martin, E.; Chen, Y.; Zhang, Z.; Sexton, K. G.; Gold, A.; Jaspers, I.; Fry, R. C.; Surratt, J. D. Isoprene-Derived Secondary Organic Aerosol Induces the Expression of Oxidative Stress Response Genes in Human Lung Cells. *Environ. Sci. Technol. Lett.* **2016**, *3* (6), 250−254.
(32) Khan, F.; Chen, Y.; Hartwell, H. J.; Yan, J.; Lin, Y.-H.; Freedman, A.; Zhang, Z.; Zhang, Y.; Lambe, A. T.; Turpin, B. J.; Gold, A.; Ault, A. P.; Szmigielski, R.; Fry, R. C.; Surratt, J. D. Heterogeneous Oxidation Products of Fine Particulate Isoprene Epoxydiol-Derived Methyltetrol Sulfates Increase Oxidative Stress and Inflammatory Gene Responses in Human Lung Cells. *Chem. Res. Toxicol.* **2023**, *36* (11), 1814−1825.
(33) Zhang, Y.-Q.; Ding, X.; He, Q.-F.; Wen, T.-X.; Wang, J.-Q.; Yang, K.; Jiang, H.; Cheng, Q.; Liu, P.; Wang, Z.-R.; He, Y.-F.; Hu, W.-W.; Wang, Q.-Y.; Xin, J.-Y.; Wang, Y.-S.; Wang, X.-M. Observational Insights into Isoprene Secondary Organic Aerosol Formation through the Epoxide Pathway at Three Urban Sites from Northern to Southern China. *Environ. Sci. Technol.* **2022**, *56* (8), 4795−4805.
(34) Bryant, D. J.; Nelson, B. S.; Swift, S. J.; Budisulistiorini, S. H.; Drysdale, W. S.; Vaughan, A. R.; Newland, M. J.; Hopkins, J. R.; Cash, J. M.; Langford, B.; Nemitz, E.; Acton, W. J. F.; Hewitt, C. N.; Mandal, T.; Gurjar, B. R.; Gadi, R.; Lee, J. D.; Rickard, A. R.; Hamilton, J. F. Biogenic and anthropogenic sources of isoprene and monoterpenes and their secondary organic aerosol in Delhi, India. *Atmos. Chem. Phys.* **2023**, *23* (1), 61−83.
(35) Karambelas, A.; Pye, H. O. T.; Budisulistiorini, S. H.; Surratt, J. D.; Pinder, R. W. Contribution of Isoprene Epoxydiol to Urban Organic Aerosol: Evidence from Modeling and Measurements. *Environ. Sci. Technol. Lett.* **2014**, *1* (6), 278−283.
(36) Budisulistiorini, S. H.; Canagaratna, M. R.; Croteau, P. L.; Marth, W. J.; Baumann, K.; Edgerton, E. S.; Shaw, S. L.; Knipping, E. M.; Worsnop, D. R.; Jayne, J. T.; Gold, A.; Surratt, J. D. Real-Time Continuous Characterization of Secondary Organic Aerosol Derived from Isoprene Epoxydiols in Downtown Atlanta, Georgia, Using the Aerodyne Aerosol Chemical Speciation Monitor. *Environ. Sci. Technol.* **2013**, *47* (11), 5686−5694.
(37) Kota, S. H.; Schade, G.; Estes, M.; Boyer, D.; Ying, Q. Evaluation of MEGAN predicted biogenic isoprene emissions at urban locations in Southeast Texas. *Atmos. Environ.* **2015**, *110*, 54−64.
(38) Pye, H. O. T.; Ward-Caviness, C. K.; Murphy, B. N.; Appel, K. W.; Seltzer, K. M. Secondary organic aerosol association with cardiorespiratory disease mortality in the United States. *Nat. Commun.* **2021**, *12* (1), 7215.
(39) Pye, H. O. T.; Appel, K. W.; Seltzer, K. M.; Ward-Caviness, C. K.; Murphy, B. N. Human-Health Impacts of Controlling Secondary Air Pollution Precursors. *Environ. Sci. Technol. Lett.* **2022**, *9* (2), 96−101.
(40) Xu, L.; Guo, H.; Boyd, C. M.; Klein, M.; Bougiatioti, A.; Cerully, K. M.; Hite, J. R.; Isaacman-VanWertz, G.; Kreisberg, N. M.; Knote, C.; Olson, K.; Koss, A.; Goldstein, A. H.; Hering, S. V.; de Gouw, J.; Baumann, K.; Lee, S.-H.; Nenes, A.; Weber, R. J.; Ng, N. L. Effects of anthropogenic emissions on aerosol formation from isoprene and monoterpenes in the southeastern United States. *Proc. Natl. Acad. Sci. U. S. A.* **2015**, *112* (1), 37−42.
(41) Riva, M.; Chen, Y.; Zhang, Y.; Lei, Z.; Olson, N. E.; Boyer, H. C.; Narayan, S.; Yee, L. D.; Green, H. S.; Cui, T.; Zhang, Z.; Baumann, K.; Fort, M.; Edgerton, E.; Budisulistiorini, S. H.; Rose, C. A.; Ribeiro, I. O.; e Oliveira, R. L.; dos Santos, E. O.; Machado, C. M. D.; Szopa, S.; Zhao, Y.; Alves, E. G.; de Sá, S. S.; Hu, W.; Knipping, E. M.; Shaw, S. L.; Duvoisin Junior, S.; de Souza, R. A. F.; Palm, B. B.; Jimenez, J.-L.; Glasius, M.; Goldstein, A. H.; Pye, H. O. T.; Gold, A.; Turpin, B. J.; Vizuete, W.; Martin, S. T.; Thornton, J. A.; Dutcher, C.

https://doi.org/10.1021/acsestair.4c00048
ACS EST Air 2024, 1, 1037−1052

S.; Ault, A. P.; Surratt, J. D. Increasing Isoprene Epoxydiol-to-Inorganic Sulfate Aerosol Ratio Results in Extensive Conversion of Inorganic Sulfate to Organosulfur Forms: Implications for Aerosol Physicochemical Properties. *Environ. Sci. Technol.* **2019**, *53* (15), 8682−8694.
(42) Stone, E. A.; Hedman, C. J.; Zhou, J.; Mieritz, M.; Schauer, J. J. Insights into the nature of secondary organic aerosol in Mexico City during the MILAGRO experiment 2006. *Atmos. Environ.* **2010**, *44* (3), 312−319.
(43) Olson, C. N.; Galloway, M. M.; Yu, G.; Hedman, C. J.; Lockett, M. R.; Yoon, T.; Stone, E. A.; Smith, L. M.; Keutsch, F. N. Hydroxycarboxylic Acid-Derived Organosulfates: Synthesis, Stability, and Quantification in Ambient Aerosol. *Environ. Sci. Technol.* **2011**, *45* (15), 6468−6474.
(44) Dzepina, K.; Volkamer, R. M.; Madronich, S.; Tulet, P.; Ulbrich, I. M.; Zhang, Q.; Cappa, C. D.; Ziemann, P. J.; Jimenez, J. L. Evaluation of recently-proposed secondary organic aerosol models for a case study in Mexico City. *Atmos. Chem. Phys.* **2009**, *9* (15), 5681−5709.
(45) Dominguez-Taylor, P.; Ruiz-Suarez, L. G.; Rosas-Perez, I.; Hernández-Solis, J. M.; Steinbrecher, R. Monoterpene and isoprene emissions from typical tree species in forests around Mexico City. *Atmos. Environ.* **2007**, *41* (13), 2780−2790.
(46) Bondy, A. L.; Bonanno, D.; Moffet, R. C.; Wang, B.; Laskin, A.; Ault, A. P. The diverse chemical mixing state of aerosol particles in the southeastern United States. *Atmos. Chem. Phys.* **2018**, *18* (16), 12595−12612.
(47) Riemer, N.; Ault, A. P.; West, M.; Craig, R. L.; Curtis, J. H. Aerosol Mixing State: Measurements, Modeling, and Impacts. *Rev. Geophys.* **2019**, *57* (2), 187−249.
(48) Olson, N. E.; Xiao, Y.; Lei, Z.; Ault, A. P. Simultaneous Optical Photothermal Infrared (O-PTIR) and Raman Spectroscopy of Submicrometer Atmospheric Particles. *Anal. Chem.* **2020**, *92* (14), 9932−9939.
(49) Ault, A. P.; Zhao, D.; Ebben, C. J.; Tauber, M. J.; Geiger, F. M.; Prather, K. A.; Grassian, V. H. Raman microspectroscopy and vibrational sum frequency generation spectroscopy as probes of the bulk and surface compositions of size-resolved sea spray aerosol particles. *Phys. Chem. Chem. Phys.* **2013**, *15* (17), 6206−6214.
(50) Ebben, C. J.; Ault, A. P.; Ruppel, M. J.; Ryder, O. S.; Bertram, T. H.; Grassian, V. H.; Prather, K. A.; Geiger, F. M. Size-Resolved Sea Spray Aerosol Particles Studied by Vibrational Sum Frequency Generation. *J. Phys. Chem. A* **2013**, *117* (30), 6589−6601.
(51) Craig, R. L.; Bondy, A. L.; Ault, A. P. Computer-controlled Raman microspectroscopy (CC-Raman): A method for the rapid characterization of individual atmospheric aerosol particles. *Aerosol Sci. Technol.* **2017**, *51* (9), 1099−1112.
(52) Fankhauser, A. M.; Lei, Z.; Daley, K. R.; Xiao, Y.; Zhang, Z.; Gold, A.; Ault, B. S.; Surratt, J. D.; Ault, A. P. Acidity-Dependent Atmospheric Organosulfate Structures and Spectra: Exploration of Protonation State Effects via Raman and Infrared Spectroscopies Combined with Density Functional Theory. *J. Phys. Chem. A* **2022**, *126* (35), 5974−5984.
(53) Ault, A. P.; Waters, C. M. Scratching the Surface of Individual Aerosol Particle Properties. *ACS Cent. Sci.* **2023**, *9* (11), 2009−2011.
(54) Bauer, S. E.; Ault, A.; Prather, K. A. Evaluation of aerosol mixing state classes in the GISS modelE-MATRIX climate model using single-particle mass spectrometry measurements. *J. Geophys. Res.: Atmos.* **2013**, *118* (17), 9834−9844.
(55) Ault, A. P. Aerosol Acidity: Novel Measurements and Implications for Atmospheric Chemistry. *Acc. Chem. Res.* **2020**, *53* (9), 1703−1714.
(56) Garzón, J. P.; Huertas, J. I.; Magaña, M.; Huertas, M. E.; Cárdenas, B.; Watanabe, T.; Maeda, T.; Wakamatsu, S.; Blanco, S. Volatile organic compounds in the atmosphere of Mexico City. *Atmos. Environ.* **2015**, *119*, 415−429.
(57) Sosa Echeverría, R.; Alarcón Jiménez, A. L.; Torres Barrera, M. d. C.; Sánchez Alvarez, P.; Granados Hernandez, E.; Vega, E.; Jaimes Palomera, M.; Retama, A.; Gay, D. A. Nitrogen and sulfur compounds in ambient air and in wet atmospheric deposition at Mexico city metropolitan area. *Atmos. Environ.* **2023**, *292*, 119411.
(58) Laskina, O.; Morris, H. S.; Grandquist, J. R.; Estillore, A. D.; Stone, E. A.; Grassian, V. H.; Tivanski, A. V. Substrate-Deposited Sea Spray Aerosol Particles: Influence of Analytical Method, Substrate, and Storage Conditions on Particle Size, Phase, and Morphology. *Environ. Sci. Technol.* **2015**, *49* (22), 13447−53.
(59) Cui, T.; Green, H. S.; Selleck, P. W.; Zhang, Z.; O'Brien, R. E.; Gold, A.; Keywood, M.; Kroll, J. H.; Surratt, J. D. Chemical Characterization of Isoprene- and Monoterpene-Derived Secondary Organic Aerosol Tracers in Remote Marine Aerosols over a Quarter Century. *ACS Earth Space Chem.* **2019**, *3* (6), 935−946.
(60) Shen, H.; Peters, T. M.; Casuccio, G. S.; Lersch, T. L.; West, R. R.; Kumar, A.; Kumar, N.; Ault, A. P. Elevated Concentrations of Lead in Particulate Matter on the Neighborhood-Scale in Delhi, India As Determined by Single Particle Analysis. *Environ. Sci. Technol.* **2016**, *50* (10), 4961−4970.
(61) Laskin, A.; Iedema, M. J.; Cowin, J. P. Quantitative Time-Resolved Monitoring of Nitrate Formation in Sea Salt Particles Using a CCSEM/EDX Single Particle Analysis. *Environ. Sci. Technol.* **2002**, *36* (23), 4948−4955.
(62) Laskin, A.; Cowin, J. P.; Iedema, M. J. Analysis of individual environmental particles using modern methods of electron microscopy and X-ray microanalysis. *J. Electron Spectrosc. Relat. Phenom.* **2006**, *150* (2-3), 260−274.
(63) Casuccio, G. S.; Schlaegle, S. F.; Lersch, T. L.; Huffman, G. P.; Chen, Y.; Shah, N. Measurement of fine particulate matter using electron microscopy techniques. *Fuel Process. Technol.* **2004**, *85* (6-7), 763−779.
(64) Ault, A. P.; Peters, T. M.; Sawvel, E. J.; Casuccio, G. S.; Willis, R. D.; Norris, G. A.; Grassian, V. H. Single-Particle SEM-EDX Analysis of Iron-Containing Coarse Particulate Matter in an Urban Environment: Sources and Distribution of Iron within Cleveland, Ohio. *Environ. Sci. Technol.* **2012**, *46* (8), 4331−4339.
(65) Casuccio, G. S.; Janocko, P. B.; Lee, R. J.; Kelly, J. F.; Dattner, S. L.; Mgebroff, J. S. The Use of Computer Controlled Scanning Electron Microscopy in Environmental Studies. *Journal of the Air Pollution Control Association* **1983**, *33* (10), 937−943.
(66) Mirrielees, J. A.; Kirpes, R. M.; Haas, S. M.; Rauschenberg, C. D.; Matrai, P. A.; Remenapp, A.; Boschi, V. L.; Grannas, A. M.; Pratt, K. A.; Ault, A. P. Probing Individual Particles Generated at the Freshwater-Seawater Interface through Combined Raman, Photothermal Infrared, and X-ray Spectroscopic Characterization. *ACS Meas. Sci. Au* **2022**, *2* (6), 605−619.
(67) Sawvel, E. J.; Willis, R.; West, R. R.; Casuccio, G. S.; Norris, G.; Kumar, N.; Hammond, D.; Peters, T. M. Passive sampling to capture the spatial variability of coarse particles by composition in Cleveland, OH. *Atmos. Environ.* **2015**, *105*, 61−69.
(68) Chen, Y.; Zhang, Y.; Lambe, A. T.; Xu, R.; Lei, Z.; Olson, N. E.; Zhang, Z.; Szalkowski, T.; Cui, T.; Vizuete, W.; Gold, A.; Turpin, B. J.; Ault, A. P.; Chan, M. N.; Surratt, J. D. Heterogeneous Hydroxyl Radical Oxidation of Isoprene-Epoxydiol-Derived Methyltetrol Sulfates: Plausible Formation Mechanisms of Previously Unexplained Organosulfates in Ambient Fine Aerosols. *Environ. Sci. Technol. Lett.* **2020**, *7* (7), 460−468.
(69) Stein, A. F.; Draxler, R. R.; Rolph, G. D.; Stunder, B. J. B.; Cohen, M. D.; Ngan, F. NOAA's HYSPLIT Atmospheric Transport and Dispersion Modeling System. *Bull. of the Am. Meteorol. Soc.* **2015**, *96* (12), 2059−2077.
(70) Teng, A. P.; Crounse, J. D.; Wennberg, P. O. Isoprene Peroxy Radical Dynamics. *J. Am. Chem. Soc.* **2017**, *139* (15), 5367−5377.
(71) Wang, M.; Hu, T.; Wu, F.; Duan, J.; Song, Y.; Zhu, Y.; Xue, C.; Zhang, N.; Zhang, D. Characterization of PM2.5 Carbonaceous Particles with a High-Efficiency SEM: A Case Study at a Suburban Area of Xi'an. *Aerosol Sci. Eng.* **2021**, *5* (1), 70−80.
(72) Zhao, P.; Zhao, P.; Tang, J.; Casuccio, G. S.; Gao, J.; Li, J.; He, Y.; Li, M.; Feng, Y. Source identification and apportionment of ambient particulate matter in Beijing using an advanced computer-

https://doi.org/10.1021/acsestair.4c00048
ACS EST Air 2024, 1, 1037−1052

controlled scanning electron microscopy (CCSEM) system. *Sci. Total Environ* **2023**, *861*, 160608.
(73) Ebert, M.; Müller-Ebert, D.; Benker, N.; Weinbruch, S. Source apportionment of aerosol particles near a steel plant by electron microscopy. *J. of Environ. Monit.* **2012**, *14* (12), 3257.
(74) Axson, J. L.; Shen, H.; Bondy, A. L.; Landry, C. C.; Welz, J.; Creamean, J. M.; Ault, A. P. Transported Mineral Dust Deposition Case Study at a Hydrologically Sensitive Mountain Site: Size and Composition Shifts in Ambient Aerosol and Snowpack. *Aerosol Air Qual. Res.* **2016**, *16* (3), 555−567.
(75) Byeon, S.-H.; Willis, R.; Peters, T. Chemical Characterization of Outdoor and Subway Fine (PM2.5-1.0) and Coarse (PM10-2.5) Particulate Matter in Seoul (Korea) by Computer-Controlled Scanning Electron Microscopy (CCSEM). *Int. J. Environ. Res. Public Health* **2015**, *12* (2), 2090−2104.
(76) Huffman, J. A.; Sinha, B.; Garland, R. M.; Snee-Pollmann, A.; Gunthe, S. S.; Artaxo, P.; Martin, S. T.; Andreae, M. O.; Pöschl, U. Size distributions and temporal variations of biological aerosol particles in the Amazon rainforest characterized by microscopy and real-time UV-APS fluorescence techniques during AMAZE-08. *Atmos. Chem. Phys.* **2012**, *12* (24), 11997−12019.
(77) Sobanska, S.; Falgayrac, G.; Rimetz-Planchon, J.; Perdrix, E.; Bremard, C.; Barbillat, J. Resolving the internal structure of individual atmospheric aerosol particle by the combination of Atomic Force Microscopy, ESEM-EDX, Raman and ToF-SIMS imaging. *Microchem J.* **2014**, *114*, 89−98.
(78) Bondy, A. L.; Kirpes, R. M.; Merzel, R. L.; Pratt, K. A.; Banaszak Holl, M. M.; Ault, A. P. Atomic Force Microscopy-Infrared Spectroscopy of Individual Atmospheric Aerosol Particles: Subdiffraction Limit Vibrational Spectroscopy and Morphological Analysis. *Anal. Chem.* **2017**, *89* (17), 8594−8598.
(79) Kirpes, R. M.; Lei, Z.; Fraund, M.; Gunsch, M. J.; May, N. W.; Barrett, T. E.; Moffett, C. E.; Schauer, A. J.; Alexander, B.; Upchurch, L. M.; China, S.; Quinn, P. K.; Moffet, R. C.; Laskin, A.; Sheesley, R. J.; Pratt, K. A.; Ault, A. P. Solid organic-coated ammonium sulfate particles at high relative humidity in the summertime Arctic atmosphere. *Proc. Natl. Acad. Sci. U. S. A.* **2022**, *119* (14), e2104496119.
(80) Kirpes, R. M.; Bondy, A. L.; Bonanno, D.; Moffet, R. C.; Wang, B.; Laskin, A.; Ault, A. P.; Pratt, K. A. Secondary sulfate is internally mixed with sea spray aerosol and organic aerosol in the winter Arctic. *Atmos. Chem. Phys.* **2018**, *18* (6), 3937−3949.
(81) Gunsch, M. J.; Liu, J.; Moffett, C. E.; Sheesley, R. J.; Wang, N.; Zhang, Q.; Watson, T. B.; Pratt, K. A. Diesel Soot and Amine-Containing Organic Sulfate Aerosols in an Arctic Oil Field. *Environ. Sci. Technol.* **2020**, *54* (1), 92−101.
(82) Zhang, R.; Khalizov, A. F.; Pagels, J.; Zhang, D.; Xue, H.; McMurry, P. H. Variability in morphology, hygroscopicity, and optical properties of soot aerosols during atmospheric processing. *Proc. Natl. Acad. Sci. U. S. A.* **2008**, *105* (30), 10291−10296.
(83) Johnson, K. S.; De Foy, B.; Zuberi, B.; Molina, L. T.; Molina, M. J.; Xie, Y.; Laskin, A.; Shutthanandan, V. Aerosol composition and source apportionment in the Mexico City Metropolitan Area with PIXE/PESA/STIM and multivariate analysis. *Atmos. Chem. Phys.* **2006**, *6* (12), 4591−4600.
(84) Vega, E.; Mugica, V.; Reyes, E.; Sanchez, G.; Chow, J. C.; Watson, J. G. Chemical composition of fugitive dust emitters in Mexico City. *Atmos. Environ.* **2001**, *35*, 4033−4039.
(85) Spencer, M. T.; Shields, L. G.; Sodeman, D. A.; Toner, S. M.; Prather, K. A. Comparison of oil and fuel particle chemical signatures with particle emissions from heavy and light duty vehicles. *Atmos. Environ.* **2006**, *40* (27), 5224−5235.
(86) Lei, Z.; Chen, Y.; Zhang, Y.; Cooke, M. E.; Ledsky, I. R.; Armstrong, N. C.; Olson, N. E.; Zhang, Z.; Gold, A.; Surratt, J. D.; Ault, A. P. Initial pH Governs Secondary Organic Aerosol Phase State and Morphology after Uptake of Isoprene Epoxydiols (IEPOX). *Environ. Sci. Technol.* **2022**, *56* (15), 10596−10607.
(87) Sadezky, A.; Muckenhuber, H.; Grothe, H.; Niessner, R.; Pöschl, U. Raman microspectroscopy of soot and related carbonaceous materials: Spectral analysis and structural information. *Carbon* **2005**, *43* (8), 1731−1742.
(88) Herdman, J. D.; Connelly, B. C.; Smooke, M. D.; Long, M. B.; Miller, J. H. A comparison of Raman signatures and laser-induced incandescence with direct numerical simulation of soot growth in non-premixed ethylene/air flames. *Carbon* **2011**, *49* (15), 5298−5311.
(89) Le, K. C.; Lefumeux, C.; Bengtsson, P.-E.; Pino, T. Direct observation of aliphatic structures in soot particles produced in low-pressure premixed ethylene flames via online Raman spectroscopy. *Proc. Combust. Inst.* **2019**, *37* (1), 869−876.
(90) Le, K. C.; Lefumeux, C.; Pino, T. Watching soot inception via online Raman spectroscopy. *Combust. Flame* **2022**, *236*, 111817.
(91) Bondy, A. L.; Craig, R. L.; Zhang, Z.; Gold, A.; Surratt, J. D.; Ault, A. P. Isoprene-Derived Organosulfates: Vibrational Mode Analysis by Raman Spectroscopy, Acidity-Dependent Spectral Modes, and Observation in Individual Atmospheric Particles. *J. Phys. Chem. A* **2018**, *122* (1), 303−315.
(92) Lin, Y.-H.; Zhang, Z.; Docherty, K. S.; Zhang, H.; Budisulistiorini, S. H.; Rubitschun, C. L.; Shaw, S. L.; Knipping, E. M.; Edgerton, E. S.; Kleindienst, T. E.; Gold, A.; Surratt, J. D. Isoprene Epoxydiols as Precursors to Secondary Organic Aerosol Formation: Acid-Catalyzed Reactive Uptake Studies with Authentic Compounds. *Environ. Sci. Technol.* **2012**, *46* (1), 250−258.
(93) Eddingsaas, N. C.; VanderVelde, D. G.; Wennberg, P. O. Kinetics and Products of the Acid-Catalyzed Ring-Opening of Atmospherically Relevant Butyl Epoxy Alcohols. *J. Phys. Chem. A* **2010**, *114* (31), 8106−8113.
(94) Gaston, C. J.; Riedel, T. P.; Zhang, Z. F.; Gold, A.; Surratt, J. D.; Thornton, J. A. Reactive Uptake of an Isoprene-Derived Epoxydiol to Submicron Aerosol Particles. *Environ. Sci. Technol.* **2014**, *48* (19), 11178−11186.
(95) Lin, Y. H.; Zhang, Z. F.; Docherty, K. S.; Zhang, H. F.; Budisulistiorini, S. H.; Rubitschun, C. L.; Shaw, S. L.; Knipping, E. M.; Edgerton, E. S.; Kleindienst, T. E.; Gold, A.; Surratt, J. D. Isoprene Epoxydiols as Precursors to Secondary Organic Aerosol Formation: Acid-Catalyzed Reactive Uptake Studies with Authentic Compounds. *Environ. Sci. Technol.* **2012**, *46* (1), 250−258.
(96) Kanellopoulos, P. G.; Kotsaki, S. P.; Chrysochou, E.; Koukoulakis, K.; Zacharopoulos, N.; Philippopoulos, A.; Bakeas, E. PM(2.5)-bound organosulfates in two Eastern Mediterranean cities: The dominance of isoprene organosulfates. *Chemosphere* **2022**, *297*, 134103.
(97) Hettiyadura, A. P. S.; Al-Naiema, I. M.; Hughes, D. D.; Fang, T.; Stone, E. A. Organosulfates in Atlanta, Georgia: anthropogenic influences on biogenic secondary organic aerosol formation. *Atmos. Chem. Phys.* **2019**, *19* (5), 3191−3206.
(98) Hughes, D. D.; Christiansen, M. B.; Milani, A.; Vermeuel, M. P.; Novak, G. A.; Alwe, H. D.; Dickens, A. F.; Pierce, R. B.; Millet, D. B.; Bertram, T. H.; Stanier, C. O.; Stone, E. A. PM2.5 chemistry, organosulfates, and secondary organic aerosol during the 2017 Lake Michigan Ozone Study. *Atmos. Environ.* **2021**, *244*, 117939.
(99) Hodzic, A.; Jimenez, J. L.; Madronich, S.; Aiken, A. C.; Bessagnet, B.; Curci, G.; Fast, J.; Lamarque, J. F.; Onasch, T. B.; Roux, G.; Schauer, J. J.; Stone, E. A.; Ulbrich, I. M. Modeling organic aerosols during MILAGRO: importance of biogenic secondary organic aerosols. *Atmos. Chem. Phys.* **2009**, *9* (18), 6949−6981.
(100) Guenther, A. B.; Jiang, X.; Heald, C. L.; Sakulyanontvittaya, T.; Duhl, T.; Emmons, L. K.; Wang, X. The Model of Emissions of Gases and Aerosols from Nature version 2.1 (MEGAN2.1): an extended and updated framework for modeling biogenic emissions. *Geoscientific Model Development* **2012**, *5* (6), 1471−1492.
(101) Jo, D. S.; Hodzic, A.; Emmons, L. K.; Marais, E. A.; Peng, Z.; Nault, B. A.; Hu, W.; Campuzano-Jost, P.; Jimenez, J. L. A simplified parameterization of isoprene-epoxydiol-derived secondary organic aerosol (IEPOX-SOA) for global chemistry and climate models: a case study with GEOS-Chem v11-02-rc. *Geosci. Model Dev.* **2019**, *12* (7), 2983−3000.

https://doi.org/10.1021/acsestair.4c00048
ACS EST Air 2024, 1, 1037−1052

(102) Lin, Y.-H.; Zhang, H.; Pye, H. O. T.; Zhang, Z.; Marth, W. J.; Park, S.; Arashiro, M.; Cui, T.; Budisulistiorini, S. H.; Sexton, K. G.; Vizuete, W.; Xie, Y.; Luecken, D. J.; Piletic, I. R.; Edney, E. O.; Bartolotti, L. J.; Gold, A.; Surratt, J. D. Epoxide as a precursor to secondary organic aerosol formation from isoprene photooxidation in the presence of nitrogen oxides. *Proc. Natl. Acad. Sci. U. S. A.* **2013**, *110* (17), 6718−6723.
(103) Surratt, J. D.; Chan, A. W. H.; Eddingsaas, N. C.; Chan, M.; Loza, C. L.; Kwan, A. J.; Hersey, S. P.; Flagan, R. C.; Wennberg, P. O.; Seinfeld, J. H. Reactive intermediates revealed in secondary organic aerosol formation from isoprene. *Proc. Natl. Acad. Sci. U. S. A.* **2010**, *107* (15), 6640−6645.
(104) Nguyen, T. B.; Bates, K. H.; Crounse, J. D.; Schwantes, R. H.; Zhang, X.; Kjaergaard, H. G.; Surratt, J. D.; Lin, P.; Laskin, A.; Seinfeld, J. H.; Wennberg, P. O. Mechanism of the hydroxyl radical oxidation of methacryloyl peroxynitrate (MPAN) and its pathway toward secondary organic aerosol formation in the atmosphere. *Phys. Chem. Chem. Phys.* **2015**, *17* (27), 17914−26.
(105) Wennberg, P. O. Let's Abandon the "High NOx" and "Low NOx" Terminology. *ACS ES&T Air* **2024**, *1* (1), 3−4.
(106) Nguyen, T. B.; Laskin, J.; Laskin, A.; Nizkorodov, S. A. Nitrogen-containing organic compounds and oligomers in secondary organic aerosol formed by photooxidation of isoprene. *Environ. Sci. Technol.* **2011**, *45* (16), 6908−18.
(107) Paulot, F. C.; Kjaergaard, H. G.; Kürten, A.; St. Clair, J. Sm.; Seinfeld, J. H.; Wennberg, P. O.; Crounse, J. D. Unexpected Epoxide Formation in the Gas-Phase Photooxidation of Isoprene. *Science* **2009**, *325* (5941), 730−733.
(108) Rinne, H. J. I.; Guenther, A. B.; Greenberg, J. P.; Harley, P. C. Isoprene and monoterpene fluxes measured above Amazonian rainforest and their dependence on light and temperature. *Atmos. Environ.* **2002**, *36* (14), 2421−2426.
(109) Pye, H. O. T.; Nenes, A.; Alexander, B.; Ault, A. P.; Barth, M. C.; Clegg, S. L.; Collett Jr, J. L.; Fahey, K. M.; Hennigan, C. J.; Herrmann, H.; Kanakidou, M.; Kelly, J. T.; Ku, I. T.; McNeill, V. F.; Riemer, N.; Schaefer, T.; Shi, G.; Tilgner, A.; Walker, J. T.; Wang, T.; Weber, R.; Xing, J.; Zaveri, R. A.; Zuend, A. The acidity of atmospheric particles and clouds. *Atmos. Chem. Phys.* **2020**, *20* (8), 4809−4888.
(110) Hernández-López, A. E.; Miranda Martín del Campo, J.; Mugica-Álvarez, V.; Hernández-Valle, B. L.; Mejía-Ponce, L. V.; Pineda-Santamaría, J. C.; Reynoso-Cruces, S.; Mendoza-Flores, J. A.; Rozanes-Valenzuela, D. A Study of Pm2.5 Elemental Composition in Southwest Mexico City and Development of Receptor Models with Positive Matrix Factorization. *Revista Internacional de Contaminación Ambiental* **2020**, *37*, 67−88.
(111) Guerrero, F.; Alvarez-Ospina, H.; Retama, A.; López-Medina, A.; Castro, T.; Salcedo, D. Seasonal changes in the PM1 chemical composition north of Mexico City. *Atmósfera* **2017**, *30* (3), 243−258.
(112) Maldonado-Bernabé, G.; Chacalo-Hilu, A.; Nava-Bolaños, I.; Meza-Paredes, R. M.; Zaragoza-Hernández, A. Y. Changes in the Surface of Green Areas in Two City Halls of Mexico City Between 1990-2015. *Polibotánica* **2019**, *48* (24), 205−230.
(113) Gu, S.; Guenther, A.; Faiola, C. Effects of Anthropogenic and Biogenic Volatile Organic Compounds on Los Angeles Air Quality. *Environ. Sci. Technol.* **2021**, *55* (18), 12191−12201.

https://doi.org/10.1021/acsestair.4c00048
ACS EST Air 2024, 1, 1037−1052